DESIGNING OF A SMALL WEARABLE CONFORMAL PHASED ARRAY ANTENNA FOR WIRELESS COMMUNICATIONS

A Thesis
Submitted to the Graduate Faculty
of the
North Dakota State University
of Agriculture and Applied Science

By

Sayan Roy

In Partial Fulfillment of the Requirements
for the Degree of
MASTER OF SCIENCE

Major Department:
Electrical and Computer Engineering

August 2012

Fargo, North Dakota

North Dakota State University
Graduate School

Title

DESIGNING OF A SMALL WEARABLE CONFORMAL PHASED ARRAY ANTENNA

FOR WIRELESS COMMUNICATIONS

By

SAYAN ROY

The Supervisory Committee certifies that this ***disquisition*** complies with North Dakota State University's regulations and meets the accepted standards for the degree of

MASTER OF SCIENCE

SUPERVISORY COMMITTEE:

Dr. BENJAMIN D. BRAATEN
Chair

Dr. DAVID A. ROGERS

Dr. MARK SCHROEDER

Dr. ALAN DENTON

Approved:

07/09/2012
Date

Dr. RAJENDRA KATTI
Department Chair

ABSTRACT

In this thesis, a unique design of a self-adapting conformal phased-array antenna system for wireless communications is presented. The antenna system is comprised of a sensor circuit and one 1x4 printed microstrip patch antenna array on a flexible substrate with a resonant frequency of 2.47 GHz. When the performance of the antenna starts to degrade under non-planar orientation, the sensor circuitry compensates the phase of each array element of the antenna. The proposed analytical method for phase compensation has been first verified by designing an RF test platform that was used to calibrate the sensor circuitry by observing the behavior of the antenna array system on surfaces with different curvatures. In particular, this phased array antenna system was designed to be used on the surface of a spacesuit or any other flexible prototypege. This work was supported in part by the Defense Miroelectronics Activity (DMEA), NASA ND EPSCoR and DARPA/MTO.

ACKNOWLEDGMENTS

First, I would like to thank my advisor, Dr. Benjamin D. Braaten, for his continuous support, patience, and guidance in completing this research. He always supported me by providing intriguing fundamental thoughts for this research. Without his guidance, I would have never been able to complete this work.

I would also like to thank my committee members, Dr. David A. Rogers, Dr. Mark Schroeder and Dr. Alan Denton, for their continuous encouragement and support. They have taught me many things and helped me in overcoming any difficulties I had along the way in this research.

I acknowledge DMEA, NASA NDEPSCoR and DERPA/MTO for their financial support for this project.

I would especially like to thank Dr. Neil F. Chamberlain with the NASA Jet Propulsion Laboratory (JPL), California and Dr. Michael Reich with the Center for Nanoscale Science and Engineering (CNSE), Fargo for their collaboration and input on various aspects of this reseach.

Finally, I would like to thank my family for their support and understanding that I had to leave my hometown in India to pursue this work.

DEDICATION

To Ma and Baba.

TABLE OF CONTENTS

ABSTRACT iii

ACKNOWLEDGMENTS iv

DEDICATION v

LIST OF TABLES ix

LIST OF FIGURES x

CHAPTER 1. INTRODUCTION 1

1.1. History 1

1.2. Background 2

1.3. Motivation for Work 2

1.4. Proposed Work 4

CHAPTER 2. PLANAR CONFORMAL ARRAY ANTENNA 6

2.1. Introduction 6

2.2. Concept of Antenna Array 6

2.3. Phased Array Antenna 6

2.4. Functional Blocks of Phased Array Antenna 6

2.4.1. Feed Network 7

2.4.2. Phase Scanning Circuitry 7

2.5. Defining Coordinate System 8

2.6. Controlling Parameters of An Array Antenna System 9

2.6.1. Geometrical orientation of the overall array 9

2.6.2. Relative separation between the elements 9

2.6.3. Excitation amplitude of the individual element 9

2.6.4. Excitation phase of the individual element 11

2.6.5. Relative pattern of the individual element 11

2.7. Array Factor 11

2.8. Phase Steering 14
2.9. Realization of Phased Array Antenna 16
CHAPTER 3. PHASED ARRAY ANTENNA TEST PLATFORM 21
3.1. Introduction 21
3.2. Motivation for Work 21
3.3. Description of Work 21
3.3.1. Four element Antenna Array 23
3.3.2. Coaxial Cable to SMA Connectors 23
3.3.3. Four-Port Receiver RF Circuit Board 25
3.3.4. DAC Controller Circuit 31
3.3.5. LabVIEW GUI 35
3.4. S-Parameter Measurements and Scanning Properties 36
3.5. Phase Compensation and Pattern Correction Results 36
3.5.1. Analytical Work for Correction of Field Pattern of The Test Platform 36
3.5.2. Phase Compensation Results 37
3.6. Gain Calculation and Compensation Results 39
CHAPTER 4. THE FOUR ELEMENT SELFLEX ARRAY DESIGN 43
4.1. Motivation 43
4.2. Description of Work 44
4.2.1. The Resistive Sensing Circuit 44
4.2.2. 1×4 SELFLEX Array Prototype 44
4.3. S-parameter and Pattern Measurement Results 47
4.3.1. Pattern Correction of The Antenna on Wedge-Shaped Surfaces 49
4.3.2. Pattern Correction of The Antenna on Cylindrical Surfaces 49
4.4. Gain Compensation Results 51
CHAPTER 5. CONCLUSIONS 52

REFERENCES 53

APPENDIX. MATLAB CODE 57

LIST OF TABLES

Table		Page
1	Gain Shift Values for the Antenna Test Platform.	42
2	Gain Shift Values for the SELFLEX array.	51

LIST OF FIGURES

Figure		Page
1	Top-view of a rectangular microstrip antenna.	3
2	A printed single microstrip antenna.	3
3	High level block diagram of the proposed antenna system.	4
4	A printed microstrip array on planar and curved surfaces with direction of maximum radiation	5
5	Corporate feed structure for an array system.	7
6	Parallel and Series Feeds.	8
7	Defining coordinate system of an antenna array system with a point source acting as the transmitter.	10
8	A typical linear array system with variable phase shifter (shown as circular blocks) and attenuator (shown as variable resistor block) segments designed to be operated as a receiver module.	11
9	Spherical Coordinate System.	13
10	Beam of an 4-element array steered to 45°.	15
11	1x4 Microstrip patch antenna array.	17
12	Phase compensation of a linear array on a single curved surface shaped as a wedge.	17
13	Phase compensation of a linear array on a single curved surface shaped as a cylinder.	19
14	Block diagram of the proposed system.	22
15	Schematic of the antenna test platform.	22
16	Four individual microstrip patch antennas on a non-conducting surface.	23
17	a) Printed individual microstrip patch antenna with detail geometry (g = 2.0 mm, h = 35.6 mm, t = 5.5 mm, w = 43.6 mm) and b) the fabricated prototype	24
18	Conformal array made of individual microstrip patches.	24
19	Picture of the four port receiver.	25
20	Voltage Controlled Phase Shifter under test.	25
21	S_{11} of the phase shifter at 2.45 GHz.	26
22	Magnitude of S_{21} of the phase shifter at 2.45 GHz.	26
23	Normalized Phase of S_{21} of the phase shifter at 2.45 GHz.	27

24 Voltage Variable Attenuator under test. 27

25 $|S_{11}|$ of the Attenuator at 2.45 GHz. 28

26 Magnitude of S_{21} of the Attenuator at 2.45 GHz. 28

27 Phase of S_{21} of the Attenuator at 2.45 GHz. 29

28 Low Noise Amplifier under test. 29

29 $|S_{11}|$ in dB of the Amplifier from 2.4 to 2.6 GHz. 30

30 Phase of S_{21} of the Amplifier from 2.4 to 2.6 GHz. 30

31 Power Combiner under test. 32

32 $|S_{11}|$ of the Combiner at Combiner Side from 2.4 to 2.6 GHz. 32

33 $|S_{11}|$ of the Combiner at one of the branch from 2.4 to 2.6 GHz. 33

34 DAC circuitry in details. 34

35 a) Picture of the 1 x 4 antenna test platform attached to a non-conducting wedge; b) picture of the 1 x 4 antenna test platform attached to a non-conducting cylinder. 36

36 Measured S_{11} of the 1 x 4 antenna test platform. 37

37 Measured and analytical scanned patterns in the $x-z$ plane for the 1 x 4 antenna test platform on a flat surface ($\theta_b = 0^\circ$). 38

38 Measured and analytical patterns at 2.45 GHz in the x-z plane for the 1 x 4 antenna test platform on a wedge with $\theta_b = 30^\circ$. 39

39 Measured and analytical patterns at 2.45 GHz in the x-z plane for the 1 x 4 antenna test platform on a wedge with $\theta_b = 45^\circ$. 40

40 Measured and analytical patterns at 2.45 GHz in the x-z plane for the 1 x 4 antenna test platform on a cylinder with a radius of curvature of 10cm. 41

41 Schematic of the 1 x 4 Self-adapting flexible (SELFLEX) array with embedded sensor circuitry. . . 45

42 Picture of the manufactured 1 x 4 SELFLEX array prototype (g = 2.0 mm, h = 35.6 mm, m = 19.8 mm, s = 11.0 mm, t = 1.3 mm, u = 33.4 mm and w = 43.6 mm). 45

43 a) Schematic of the sensor circuit used to measure the resistance and control the phase shifters (V_{cc} = 15V, R_{gain}=4.7$k\Omega$ and $V_{ref} = -V_{cc}$ = -0.4V) and b) a picture of the flexible resistive sensor used for measuring surface deformation. 46

44 Measured output of the phase shifter controlled by the sensor circuit where θ_b is the bend angle and $\Delta\phi_n^w$ is the phase compensation for the n^{th} antenna element in the array. 46

45 Measured S_{11} of the 1 x 4 SELFLEX array for various conformal surfaces. 47

46 Measured and analytical patterns at 2.47 GHz in the x-z plane for the array with the embedded sensor circuit on a wedge with $\theta_b = 30^\circ$. 48

47 a) Picture of the 1 x 4 SELFLEX array attached to a non-conducting wedge and b) picture of the 1 x 4 SELFLEX array attached to a non-conducting cylinder. 48

48 Measured and analytical patterns at 2.47 GHz in the x-z plane for the array with the embedded sensor circuit on a wedge with $\theta_b = 45^\circ$. 49

49 Measured and analytical patterns at 2.47 GHz in the x-z plane for the array with the embedded sensor circuit on a cylinder with a radius of curvature of 10cm. 50

50 Measured calibrated gain of the 1 x 4 SELFLEX array for various conformal surfaces. 51

CHAPTER 1. INTRODUCTION

1.1. History

In the year of 1873, famous physicist James Clerk Maxwell mathematically described the nature of electromagnetic waves. In his book, "A Treaties on Electricity and Magnetism", he proposed four sets of partial differential equations that explain the quantitative and qualitative analysis on electromagnetic waves. These equations are known as Maxwells Equations and have been considered to be one of the greatest discoveries of 19th century in the world of mathematical physics. A few years later, another famous physicist Heinrich Hertz experimentally demonstrated the existence of electromagnetic waves in free space. However, it took another twenty-two years to apply the concept of Maxwells equations in practice when two scientists from two different countries, Sir Jagadish Chandra Bose from India and Guglielmo Marconi from Italy separately demonstrated the engineering behind radio waves and the usefulness of wireless communications through radio waves in the year of 1895. Afterwards, the wireless communications soon gained popularity due to two World Wars. Today wireless communications is being exploited from clinical practice to extraterrestrial communications. Space science is one of the domains that experienced a dramatic advancement after the invention of powerful antennas. Antenna is one of the basic building blocks in the world of wireless technology. The fields of antenna and wave propagation has drawn the attention of researchers for last thirty years resulting in many inventions of new types of antennas with superior performance and versatile features. Conformal antennas is one of these new types of antennas. A conformal antenna can be described as an antenna that conforms to a prescribed shape. The shape can be some part of an airplane, a spacesuit, a high-speed train or other types of physical entities. The purpose will be to build antenna systems in such a way that the antenna integration makes the antennas less disturbing yet maintaining the optimum performance [1]. Usually, a conformal antenna is cylindrical, spherical, or some other shape, with the radiating elements mounted on or integrated into the smoothly curved surface.

The IEEE Standard Definition of Terms for Antennas (IEEE Std 145-1993) gives the following definition:

2.74 conformal antenna [conformal array]. An antenna [an array] that conforms to a surface whose shape is determined by considerations other than electromagnetic; for example, aerodynamic or hydrodynamic.

1.2. Background

Antennas are used to transmit and receive electromagnetic signals in wireless communication systems. From the view of a receiving antenna, the quality of the antenna depends upon how well it can receive the faintest electromagnetic waves. In general, antennas with very large aperture can detect faint signals much better than antennas with a comparatively smaller aperture. However, a larger aperture demands bulky systems and complex construction engineering which sometime exceeds the feasibility for physical implementation of the antenna. One way to overcome this challenge is to implement antenna array concepts where a number of identical antennas with very small apertures can be cascaded in different manners based on their functionality. The output of each small antenna is then combined to enhance the total received signal that is equivalent to the signal received with a single antenna with a large aperture. Mathematically, an antenna array can offer an aperture that exceeds the aperture of a single antenna and thus it can be capable of detecting extremely faint signals from far away sources [2]. The compromised factor here is the complexity. Since the electromagnetic signals received by each antenna array element differs from the signals received by other array elements in terms of amplitude and phase, they must be combined coherently to achieve the desired output. Though it is more complex to set up an antenna array compared to a single antenna, weighting the signals before combining them enables enhanced performance features such as interference rejection and beam steering without physically moving the aperture. The trade-off for these attractive features is increased complexity and cost.

1.3. Motivation for Work

Now-a-days wireless systems are exploited in the domain of space communication, harvesting energy, tracking inventory and streaming entertainment to billions of people around the globe. The microstrip antenna shown in Fig. 1 is one of the most popular antennas used currently in wireless communications because of its simple geometry, ease of design, compactness, durability and low manufacturing cost. A more detail geometry related to the designing of a printed microstrip antenna is illustrated in Fig. 2. This type of antenna consists of a single conducting plane, usually made with copper, printed on the top layer of a dielectric material. A ground plane, also made with copper, is then printed on the bottom layer of the dielectric substrate. The radiation of the antenna can be achieved by generating an electric field between the two conductor layers of the antenna by applying a voltage between the two conductors on the top and the bottom of the substrate. Widespread use of printed microstrip antennas has drawn a lot of attention in the area of research that includes but is not limited to, ultra wide-band antennas, reconfigurable antennas, metamaterials-based antennas and millimeter-wave integrated phased arrays [3]. However, most of the geometries of the aforesaid systems are limited to

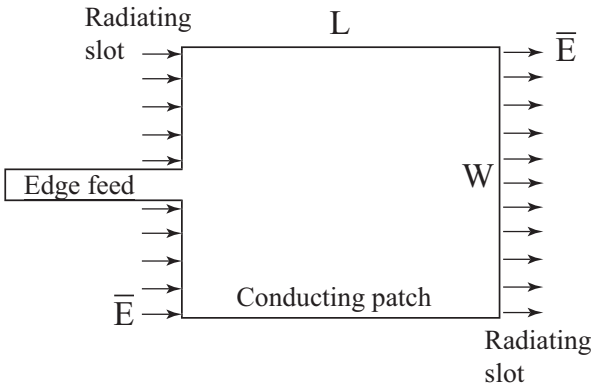

Figure 1. Top-view of a rectangular microstrip antenna.

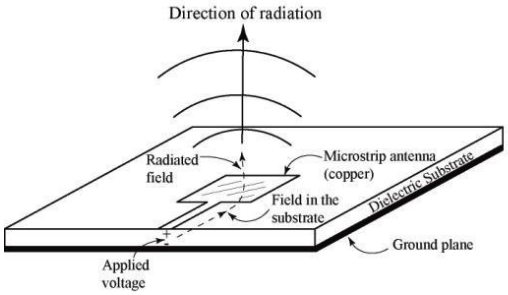

Figure 2. A printed single microstrip antenna.

planar surfaces. Therefore if a printed antenna is required to be operated on a conformal surface, then the performance may be less than desirable. One solution to design a printed microstrip antenna array on a non-planar surface is to print a planar conformal array antenna on a semi-flexible or flexible substrate capable of being mounted on a curved surface. Though several initial designs of conformal antennas have been previously proposed, most of them are limited to operation only on a particular non-planar surface with a fixed and known curvature. Therefore if an antenna system can be developed to be operated under such conditions where the change of the curvature of the surface of the antenna array is acceptable during its operation, then the system will offer more flexibility in terms of using it on a non-planar surface with different and unknown curvatures. Thus, implementation of the conformal array concepts of printed microstrip antennas on a flexible substrate can be a solution to applications that require the antenna to be used on curved surfaces that change with time.

1.4. Proposed Work

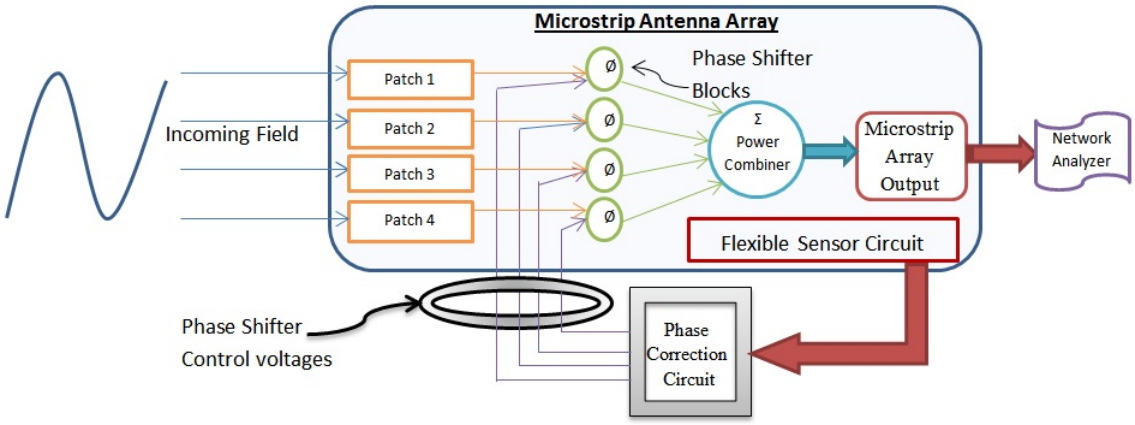

Figure 3. High level block diagram of the proposed antenna system.

One of the drawbacks of an antenna array is the lack of ability to recover the original radiation pattern when it undergoes some sort of change in its physical structure. As illustrated in Figures 4(a) and 4(b), an antenna array has the capability of changing the direction of radiation by controlling the individual phases of the voltages being supplied to each microstrip antenna array, known as beam steering. To do that, implementation of flexible sensor circuitry in a planar conformal antenna array is being proposed in this thesis. In particular, the flexible sensor circuit will be used with suitable phase compensation circuitry to dynamically determine the changes in the curvature of the antenna surface and the circuit then modifies necessary input signals to each array element through a feedback path. The block diagram of the proposed setup has been shown in Fig. 3.

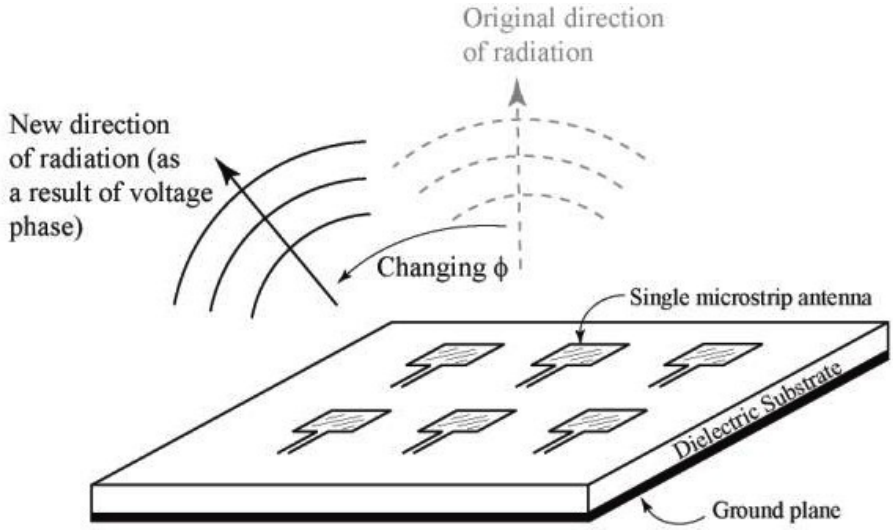

(a) A printed microstrip antenna array.

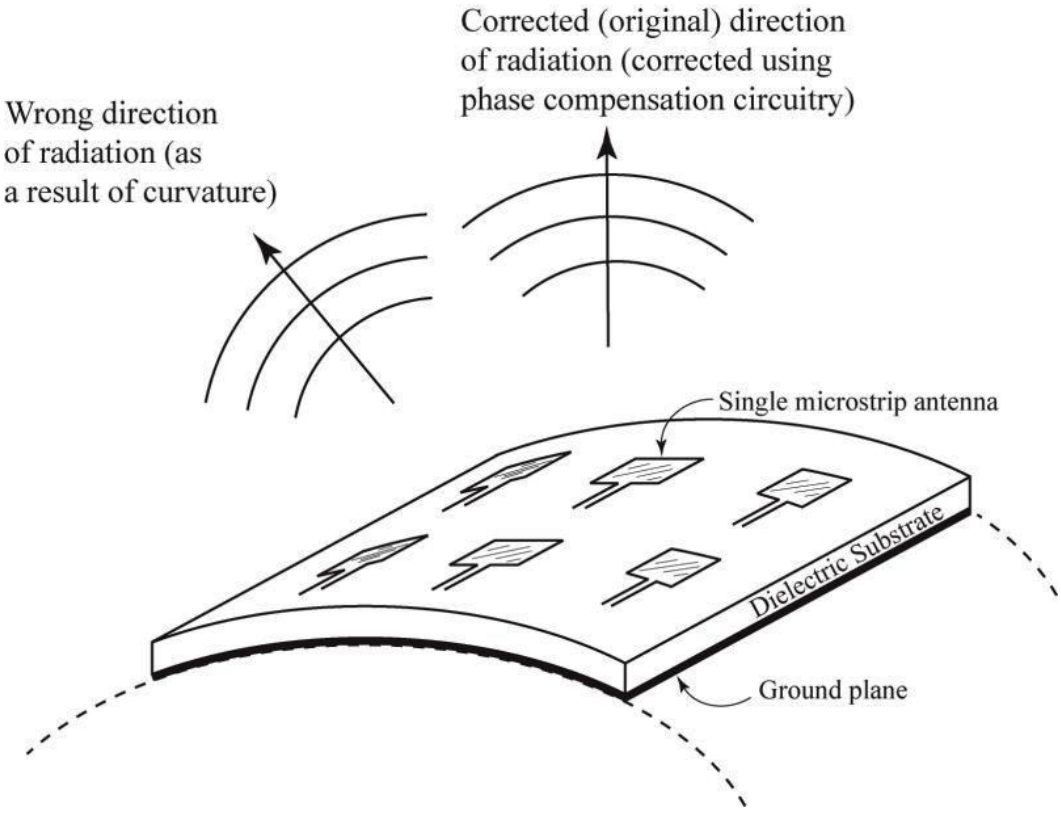

(b) A printed microstrip array on a curved surface illustrating a change in radiation direction as a result of curvature and radiation correction using phase compensation circuitry.

Figure 4. A printed microstrip array on planar and curved surfaces with direction of maximum radiation

CHAPTER 2. PLANAR CONFORMAL ARRAY ANTENNA

2.1. Introduction

This chapter presents the details involved with the conformal array antenna system. In general, conformality means preserving the correct angles within small areas, though distorting distances. Specifically for any conformal antenna, the antenna system is deployed to work on any non-planar surface in such a way that the performance of the antenna remains unchanged with respect to the performance of the antenna that has been placed on a flat surface. Particularly, the background on conformal array antenna and scanning techniques have been discussed in this chapter for a better understanding of the theory of conformal array antennas.

2.2. Concept of Antenna Array

An antenna array is a set of N antenna elements. Practically, the value of N has a range from 2 to several thousands, as in the AN/FPS-85 Phased Array Radar Facility operated by U. S. Air Force [4]. The reason why the array antenna is more popular than its equivalent single element prototype is that the array introduces the ability to scan not only the frequency band but also the coverage area without increase in size of the total system. Based on different types of spacial distributions of the elements and application of signal processing units in the array, an antenna array can offer superior performance to an individual element in terms of bandwidth and directivity [5].

The fields radiated from a linear array are a superposition of the fields radiated by each element in the presence of the other elements. Each element has an excitation parameter, which is current for a dipole, voltage for a slot and mode-voltage for a multiple-mode element. The excitation of each element will be a complex number, with amplitude and phase. This discrete distribution is called an aperture distribution where the array is the aperture.

2.3. Phased Array Antenna

One popular way to achieve electronic scanning in an antenna arrays is to feed array elements by means of phase shifters in such a way that the phase variations along the array follow an arithmetical progression whose common difference is the phase shift between two adjacent elements. Thus the array generates a plane wave whose direction depends on this phase difference [7].

2.4. Functional Blocks of Phased Array Antenna

Any phased array antenna in general, apart from the array elements, consists of two functional blocks known as feed network and phase scanning circuitry. Each of these blocks plays very important roles for the correct functionality of the array and are described here in detail.

2.4.1. Feed Network

A feed network distributes energy to the elements of the array by means of phase shifters according to a desired amplitude function. Corporate binary feed, as shown in Fig. 5 is common in arrays of dipoles, open-end guides and patches. Such feed circuits are commonly binary but can be modified to design 3-way or 5-way dividers, depending upon the number of array elements. The critical component in the corporate feed is the power divider that can be realized by bifurcated T waveguide or coaxial T junctions [6]. One challenge in design of this type of feed network is that each of the elements is required to be impedance matched and isolated or the reflected signal from each element results in a parasitic radiation pattern that will be superimposed on the required pattern. This condition plays an important role in the design of feed networks, where it is often necessary to use a directional couplar or a matched transmission line.

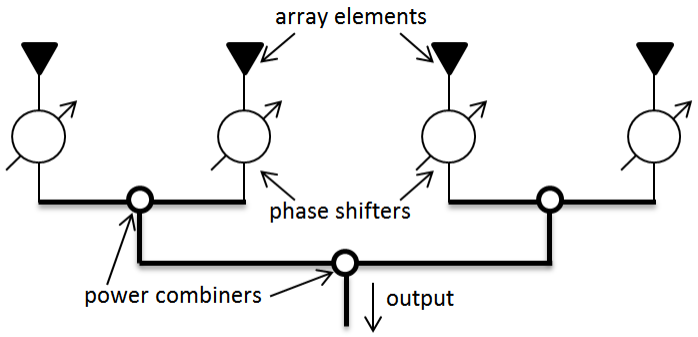

Figure 5. Corporate feed structure for an array system.

2.4.2. Phase Scanning Circuitry

One primary goal of developing phased-array antennas is to achieve beam steering electronically and thus to eliminate the mechanical movement of an antenna system. Electronic beam steering in an array antenna can be realized by time delay scanning, frequency scanning or phase scanning techniques. However, ease of implementation, cheaper digital control circuits, fast response time and high sensitivity make the phase scanning method the most popular. For proper functionality, a clever choice for a phase shifter is a switched line or ferrite phase shifter with analog or digital control. A good choice for the placement of phase shifters along the feed line is also a very important factor. The orientation may be in series or in parallel, as shown in Fig. 6. Although the series phasers have the advantage of sharing equal power, the disadvantage is the phase compensation circuit because the basic interelement phase shift must be multiplied by the number of elements and the attenuations of the phasers add up along

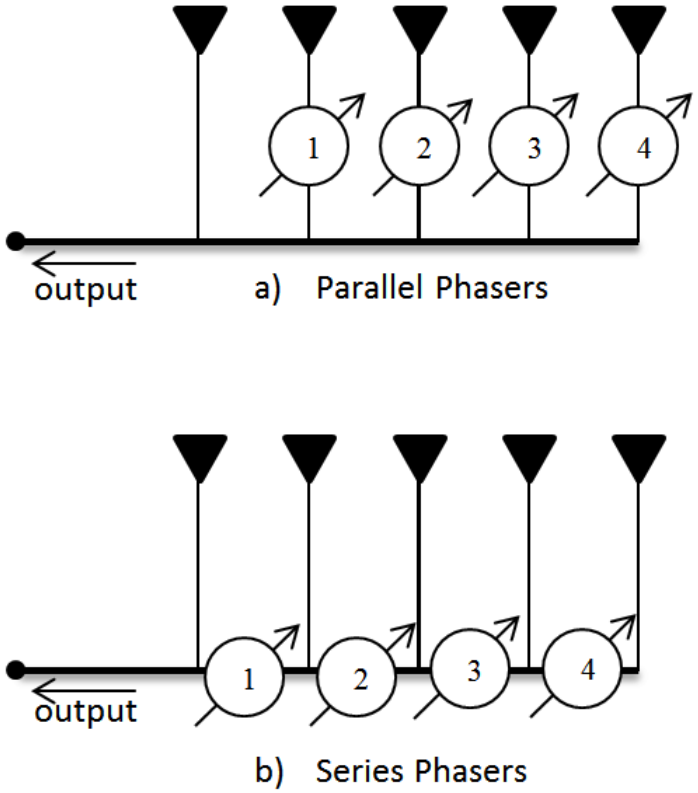

Figure 6. Parallel and Series Feeds.

the feed line. On the contrary, for parallel combination, although each phase shifter does not share the same power, the major advantage is all phasers are independent of each other and thus modeling of the control circuit becomes simpler. The mathematical approach to the phase compensation calculation will be discussed in the next section.

2.5. Defining Coordinate System

For notation purposes, henceforth it will be assumed that any linear planar array will be lying on the x-y plane with the z-axis pointing broadside to the array unless otherwise mentioned, as shown in Fig. 7(b). One objective of this project is to build an array system for a receiver, therefore any antenna system will be considered as a receiver module with respect to a point source acting as a trasmitter, as shown in Fig. 7(a). The rectangular coordinate system has been used throughout the discussion with proper notation. To define the angular separation of the array element from an axis, two parameters have been defined, denoted as the elevation angle or scan angle (θ) and the azimuthal angle (ϕ). The

scan angle has been defined as the angular separation of the elements from the broadside direction or specifically, the z axis. The azimuthal angle has been defined as the angle between the elements and x axis, as shown in Fig. 7(b). Now considering the Cartesian coordinate system, a new parameter has been defined here,

$$\Psi_n = k(x_n u + y_n v) \tag{2.1}$$

where

$$k = \frac{2\pi}{\lambda} \tag{2.2}$$

(x_n, y_n) is the location of the element n in the x-y plane, k is the wave number and

$$u = \sin\theta\cos\phi \; and \; v = \sin\theta\sin\phi \tag{2.3}$$

2.6. Controlling Parameters of An Array Antenna System

Two important properties of any individual antenna are return loss and radiation pattern. Return loss is the measurement of impedance mismatch along the path of propagation of the signal. Often termed as (S_{11}), this parameter determines the reflection coefficient (Γ) of the system. The radiation pattern or the field pattern describes the angular dependency of the strength of the radiowaves received by the antenna, usually expressed in dB (and sometimes in dBi when compared with the field pattern of an isotropic radiator). But when multiple antennas are used to form an array, as shown in Fig. 8, there are several factors that determine the behavior of the antenna array [5], and are discussed below.

2.6.1. Geometrical orientation of the overall array

The geometrical orientation of the array may be linear, planar, circular, spherical etc. in nature. When the array elements lie along a straight line, it will be denoted as a linear array and when these are located on a plane, the array will be denoted as a planar array. Depending upon the spatial distribution of the array elements, a planar array may be designed as a circular or rectangular array. However, for each of the cases, the effective field distribution and mutual coupling will be different from one another.

2.6.2. Relative separation between the elements

The relative spacing between the elements of the array determines the position of the peak and the null of the field pattern, and hence, careful choices need to be taken during the design of an array.

2.6.3. Excitation amplitude of the individual element

Amplitudes of the current on the elements of an array can be varied to shape the beam and control the level of the sidelobes of the array. This phenomenon is known as amplitude tapering and the arrays of these types are termed as *non-uniformly excited arrays* [14].

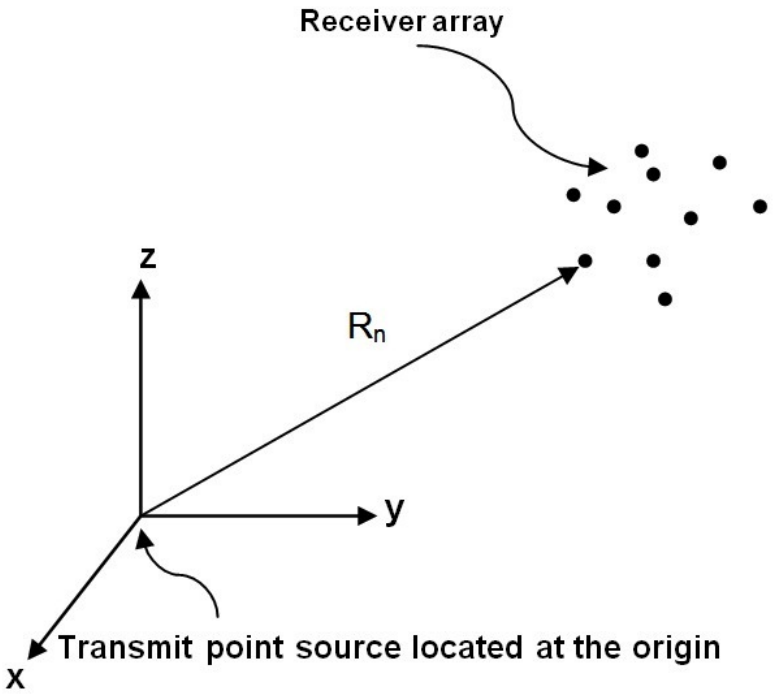

(a) Aray system with a point source transmitter.

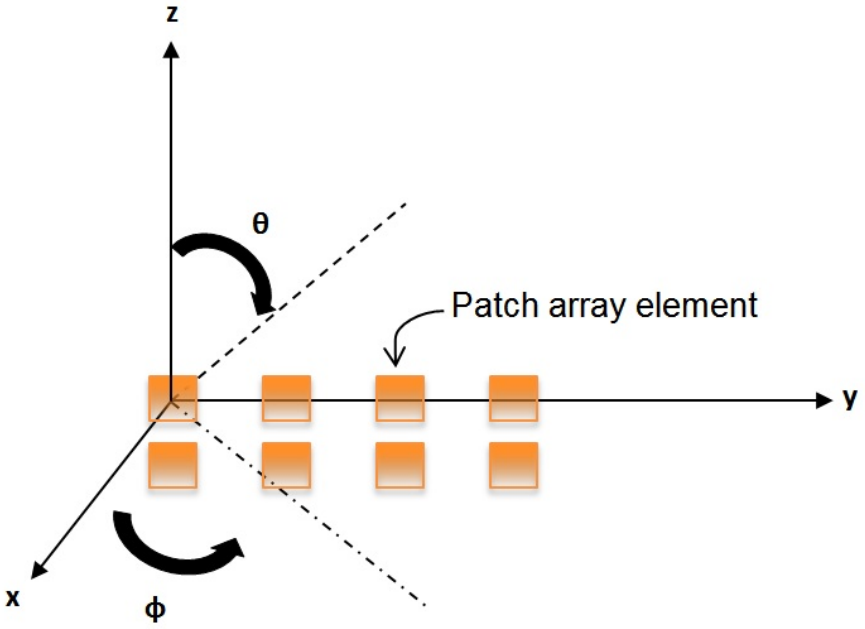

(b) Distribution of elements of a 2X4 patch antenna array on the x-y plane.

Figure 7. Defining coordinate system of an antenna array system with a point source acting as the transmitter.

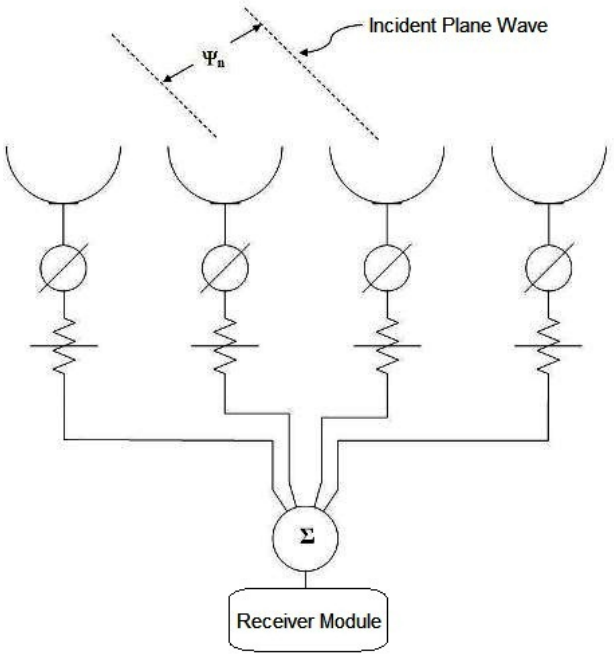

Figure 8. A typical linear array system with variable phase shifter (shown as circular blocks) and attenuator (shown as variable resistor block) segments designed to be operated as a receiver module.

2.6.4. Excitation phase of the individual element

The relative phases of the currents on each individual element of an array can be controlled to reinforce the field pattern of the array in a particular direction. These types of arrays are known as phased array antennas.

2.6.5. Relative pattern of the individual element

The overall response of the array is the superposition (sum) of all individual elements of the arrays excited separately and thus can be mathematically determined by a Fourier transformation. To avoid complexity in terms of design and calculation, generally arrays are considered to be made of identical elements.

2.7. Array Factor

An important factor related to the array antenna is the Array Factor (AF) which is unique for each array and depends on various parameters such as the number of elements of the array and their geometrical arrangements, relative magnitude, phase shift and interelement spacing. If $\mathbf{E_s}$ is the response of a single element of a linear array and if the AF is the array factor of that array, then the total response

$\mathbf{E_{total}}$ at the far-field of the array can be expressed as [5]:

$$|\mathbf{E_{total}}| = [\mathbf{E_s}][AF] \tag{2.4}$$

provided all the elements of the array are identical in nature. This concept can be used even if the actual elements are not isotropic sources. Then the total field can be determined by multiplying the array factor of the array made of isotropic sources and the field due to a single isotropic element. This concept is known as pattern multiplication and can be a very powerful tool for practical cases where elements of an array are not isotropic sources [5]. For a system where an isotropic point source is the receiver, the field of the array turns out to be proportional to the weighted sum of the received signal from each element in the array. The far-field radiation pattern is the discrete Fourier transform of the array excitation [5]. The array notation used here is θ for the angle from broadside, θ_0 being the scan angle, d for the element spacing and λ for corresponding wavelength. Mathematically [6],

$$|\mathbf{E}(x_f, y_f, z_f)| \propto \sum_{n=1}^{N} w_n \frac{e^{jkR_n}}{R_n} \tag{2.5}$$

where R_n is the distance from the element n to the point (x_f, y_f, z_f) of a rectangular coordinate system. The phase of the received signals at the element will be positive as the signal is travelling toward the element. When the array is very far from the point source, then all the R_n in the denominator of equation (2.5) are approximately the same. Consequently, the resulting field is the proportional to the sum of the weighted phase vectors and can be expressed as [6],

$$|\mathbf{E}(x_f, y_f, z_f)| \simeq \sum_{n=1}^{N} w_n e^{jkR_n} \tag{2.6}$$

Generally, arrays are either planar or linear. To make calculations easy, henceforth it will be assumed that the array elements lie along the x, y or z axes under normal condition. The phase reference or the point of zero phase can be regarded to be any element of the array. However, the origin of the coordinate system should be considered to be placed at the phase center to reduce calculations complexity. An incident plane wave arrives at all of the elements at the same time when the incedent field is normal or broadside to the array. When the plane wave is off-normal, then the plane arrives at each element at a different time. Thus, the phase difference between the signals received by the elements is accounted for an appropriate phase delay before summing the signals to get the array output [6]. For the calculation of

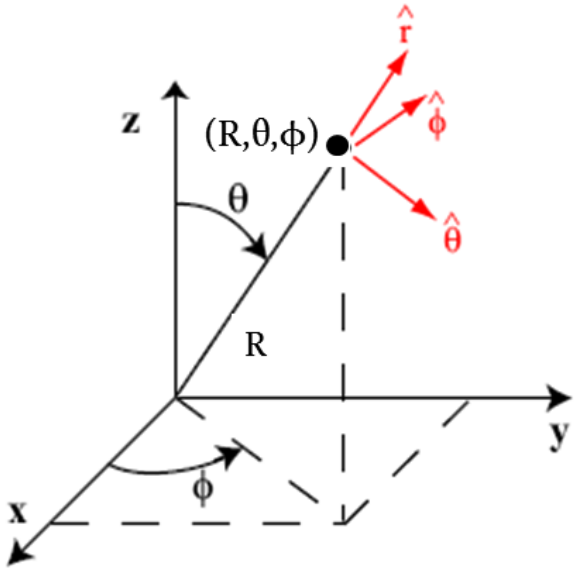

Figure 9. Spherical Coordinate System.

phase delay and array factor, Spherical coordinate system has been used here. Conversion from Spherical coordinate system to its equivalent Cartesian coordinate system has been given in equation (2.7).

Let us consider that an element is lying at (R, θ, ϕ) in a Spherical coordinate system as shown in Fig. 9. Now for any incident wave vector located on the $x-y$ plane, the phase will be a function of ϕ and for any incident wave vector located on the $y-z$ plane, the phase will be a function of θ where

$$x = R\sin\theta\cos\phi$$

$$y = R\sin\theta\sin\phi$$

$$z = R\cos\theta \tag{2.7}$$

$$R = \sqrt{x^2+y^2+z^2}$$

$$R = \tan^{-1}\left(\frac{y}{x}\right)$$

and

$$R = \cos^{-1}\left(\frac{z}{\sqrt{x^2+y^2+z^2}}\right)$$

If w_n is the complex weight factor for element n, then the array factor AF due to isotropic point sources is a weighted sum of the signals received by the elements and can be expressed as,

$$AF = \sum_{n=1}^{N} w_n e^{j\Psi_n} \tag{2.8}$$

where

$$w_n = a_n e^{j\delta n} \tag{2.9}$$

(x_n, y_n, z_n) is the location of element

(θ, ϕ) is the direction in space

and

$$\Psi_n = \begin{cases} kx_n u = kx_n \cos\phi \; or \; kx_n \sin\theta, & \text{along x axis;} \\ ky_n u = ky_n \sin\phi \; or \; ky_n \sin\theta, & \text{along y axis;} \\ kz_n \cos\theta, & \text{along z axis.} \end{cases} \tag{2.10}$$

2.8. Phase Steering

By controlling the progressive phase difference between each individual elements of an array, the field pattern of the array can be reinforced in certain directions to form a scanning array. In Fig. 10, the change of direction of maximum radiation of an array has been shown graphically. Let us assume, the maximum radiation of the array is required to be in the direction $u = u_s$. Now, the direction of maximum radiation refers to the peak of the main beam of the field pattern of the array. But, at the peak of the main beam, the array factor has the maximum value of:

$$AF_{max} = \sum_{n=1}^{N} w_n \tag{2.11}$$

Therefore, without moving the antenna physically this condition can be achieved by adding a constant phase shift δ_n to the parameter Ψ_n. Now mathematically,

$$\Psi_n = kx_n u + \delta_n \tag{2.12}$$

But according to equation (2.11), $\Psi_n = 0^\circ$ for the desired steering direction, earlier defined by $u = u_s$.

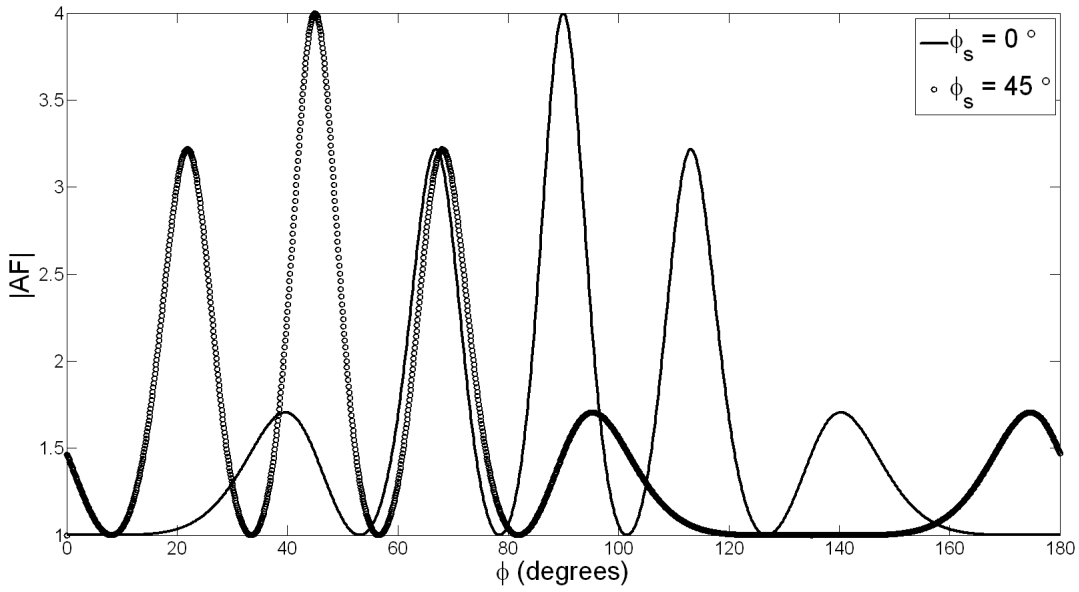

Figure 10. Beam of an 4-element array steered to $45\,^{\circ}$.

Therefore,

$$\Psi_n = (kx_n u + \delta_n)|_{u=u_s}$$

$$\Rightarrow \delta_n = -kx_n u_s \tag{2.13}$$

This is the basic principle of electronic scanning for phased array operation. Practically, continuous scanning can be realized using commercially available phase shifters which are available as either ferrite-based or diode phase shifters. However, to achieve a fixed phase difference, one can also apply the theory of path delay by introducing equivalent length of signal trace on the path of signal propagation to individual elements in the array.

For a complete discussion on this issue, let us consider a phase steering example of a phased array system consisting of 4 elements along x-axis with element spacing of 0.5λ. Now steering the beam to $45\,^{\circ}$, as shown in Fig. 10, requires a phase at element n of value δ_n where δ_n can be computed using equation (2.13) and can be expressed as,

$$\delta_n = -cos(45\,^{\circ}) \times \frac{2\pi}{\lambda} \times 0.5\lambda \times (n-1)$$

$$\Rightarrow \delta_n = -0.707\pi(n-1) \quad radians \tag{2.14}$$

The above mathematical model of the theory of phase steering can thus be validated for any array antenna system. This validation, in particular, leads to the motivation of designing a conformal array antenna. In the case of a conformal array antenna, the surface of the substrate can be changed between planar and non-planar orientations during the time of operation. Now, when the surface remains planar, the system behaves normally. However, as the surface changes to a non-planar orientation, not only the distances between the elements of the array change but also the direction of maximum radiation differs for each individual element. These changes lead to an overall distorted field pattern of the array. By using the concept of phase steering, the direction of maximum radiation of the array can then be controlled by introducing phase correction. Moreover equation (2.13) suggests that δ_n also depends on the geometrical placement of the element n, given by x_n from the origin in the Cartesian coordinate system.

2.9. Realization of Phased Array Antenna

Let us consider a 1x4 linear microstrip patch antenna array in the $x-y$ plane, as shown in Fig. 11. The array, as shown, consists of four identical microstrip rectangular patches. Therefore if the amplitude and phase of excitation current on each individual element of the array are the same, there will be no change in the behavior of the array. An angle ϕ_s has been defined here as the angle between the direction of maximum radiation and the x-axis. It is assumed that the direction of maximum radiation is broadside to the array. This angle ϕ_s is then equal to $\pi/2$ when the array elements are considered to be placed on the $x-y$ plane.

Now the main objective of this work is to rescue the radiation pattern of the conformal array during its nonplanar activity. Since broadside radiation is desired, it will be expected that the effective driving current on each individual element has to be kept equal in terms of amplitude and phase. Then only the fields radiated from each element will arrive in the same manner to any plane along the broadside direction. The two dimensional orientation of the array in both planar and nonplanar stages have been shown in Fig. 12. A circular nonplanar orientation can also be designed which will be discussed later. First we will consider correction of phase of a conformal antenna on a wedge shaped surface as shown in Fig. 12. The grey dotted line in Fig. 12 defines the position of the array in a planar orientation and the solid line defines the position of the array after bending into a non-planar orientation. The angle ϕ_s, described earlier is shown here. A new parameter θ_w has been introduced in this section to define the angular separation between the two planes of the array after bending. In practice, this situation can be realized by placing the array on a wedge with angle θ_w made up of any non-conducting material such as wood or Styrofoam. The antenna elements situated on the positive $x-$axis are denoted as A_{+n} and the elements situated on the negative $x-$axis are denoted as A_{-n} where n is the number of elements of the

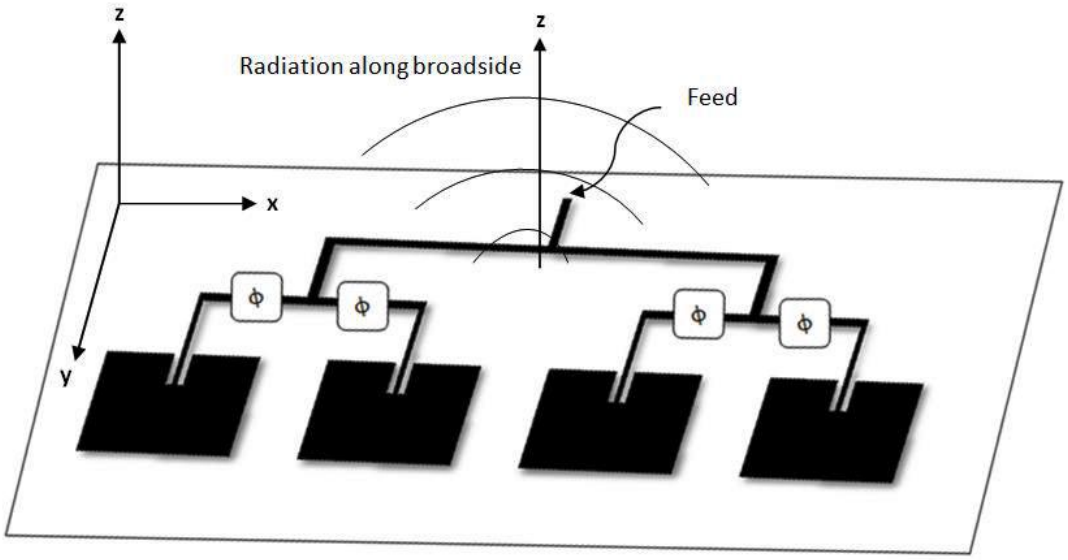

Figure 11. 1x4 Microstrip patch antenna array.

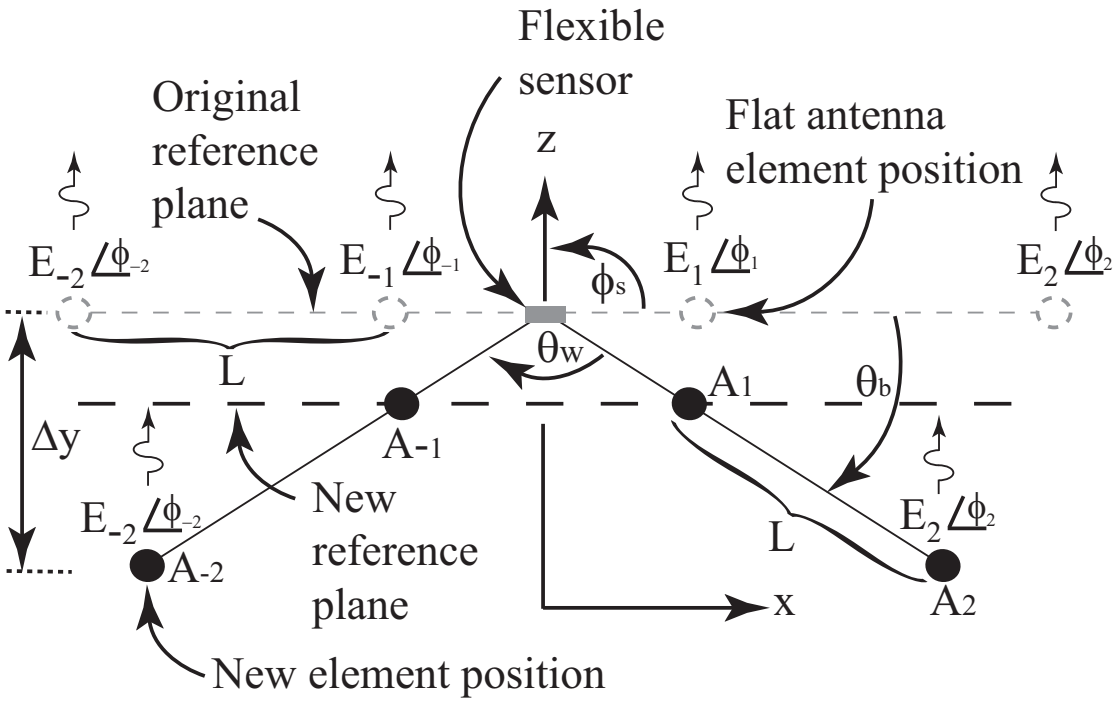

Figure 12. Phase compensation of a linear array on a single curved surface shaped as a wedge.

array with respect to the center of the array, located at the origin. The field from each element $A_{\pm n}$ has been denoted as $E_{\pm n}$. If (x_n, z_n) is the location of the n^{th} element of the linear conformal array in Fig. 12, then, for any non-planar orientation of the array, an $x-$ and $z-$translation will be incurred from the original flat position for each array element. Now, when the fields from $A_{\pm 2}$ arrive at the new reference plane, as shown in Fig. 12., they will lag the radiated fields from element $A_{\pm 1}$ due to the observation of negative phase along the propagation of the free space wave. Therefore the phases of current at $A_{\pm 2}$ should be positive enough to compensate for the phase delay introduced by that free space propagation to ensure that the fields arrive at the new reference plane with the same phase for broadside radiation. Clearly, this phase delay depends upon the angle θ_w. The amount of free-space phase introduced by the propagation of the wave from elements $A_{\pm 2}$ to the new reference plane can be computed by using the equation below [2],

$$\delta_n = -k(|x_n| \cos \phi_s + |z_n| \sin \phi_s) \tag{2.15}$$

Now as mentioned earlier, the primary concern of this work is to maintain the radiation pattern in the broadside direction. So it can be inferred that irrespective of any value for θ_w, the value of the scan angle ϕ_s will be considered to be $\pi/2$. This then simplifies equation (2.15) to

$$\delta_n = -k|z_n| \tag{2.16}$$

Next, the required phase compensation has been calculated using θ_w. Consider the case when the 1×4 array is attached to the conformal surface shown in Fig. 12. The phase of the current at each element will be different with respective to each other during receiving any signal from a transmitter at far-field. This will eventually lead to a distorted radiation pattern of the array. This can be described as follows. Under flat conditions when the array is acting as a planar array, the electric fields radiated from each antenna leave the original reference plane with the same phase to create a broadside radiation pattern. However, when the array is placed on a wedge shaped surface, situated at the origin, the geometrical orientation of the elements changes. As Fig. 12 suggests, the position of elements A_{+1} and A_{-1} now belong to a new plane, shown as the black dotted line and the position of elements A_{+2} and A_{-2} belong to another new plane. So now, when any signal from the far-field will be received by the array, the elements of the array will no longer receive the signals coherently. Mathematically, the predefined angle ϕ_s will be changed therefore for the nonplanar application of the array as the array elements will be then excited with signals with different attributes. Clearly, the signals received by $A_{\pm 2}$

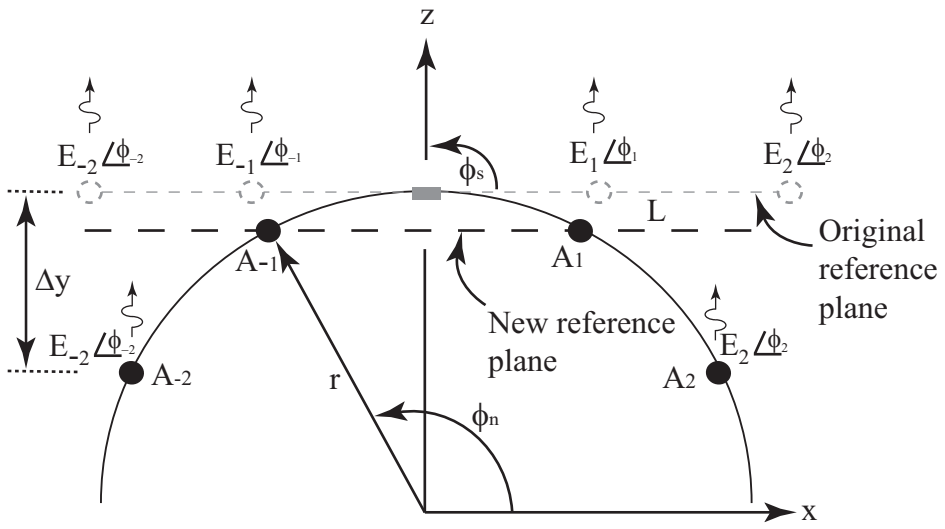

Figure 13. Phase compensation of a linear array on a single curved surface shaped as a cylinder.

have to travel a path distance more than the signals received by $A_{\pm 1}$ where this path distance is the linear separation between those two planes where the elements $A_{\pm 1}$ and $A_{\pm 2}$ are lying. From Fig. 12, this path distance can be calculated in terms of θ_w as $L\cos(\theta_w/2)$ where L is the element spacing in terms of wavelengths. Now as the path delay of an unit length affects the phase delay of any signal by its wave number, therefore for the above scenario, the resulting phase delay will be $kL\cos(\theta_w/2)$. For the discussion, let θ_b be the bend angle of the array where it can be expressed as a function of angle θ_w, given by,

$$\theta_b = \frac{(\pi - \theta_w)}{2} \tag{2.17}$$

Then the phase delay between the signals received by the elements $A_{\pm 1}$ and $A_{\pm 2}$ can be expressed in terms of θ_b as $kL\sin\theta_b$. For the plane where the elements $A_{\pm n}$ are located, the phase delay between the signals received by $A_{\pm 1}$ and $A_{\pm n}$ will be therefore $kL|n|\sin\theta_b$. As the phase has being corrected here towards the source, therefore it will be additive in nature [2]. The expression in equation (2.18) is the phase difference between the adjacent antenna elements required to correct the radiation pattern of the array placed on a wedge with a bend angle θ_b. The superscript w has been used to denote the case of wedge-shaped surface. It has been also shown in [2] that for bend angles large enough, two different main lobes from the antenna begin to appear in directions that are normal to the flat surfaces on each side of the wedge.

$$\Delta\phi_n^w = +kL|n|\sin\theta_b \tag{2.18}$$

Apart from wedge shaped surface, a conformal array can also be realized on a singly curved surface such as a cylinder. Fig. 13 describes the position of the antenna elements placed on such a cylinder of radius r with its axis aligned with $z-$axis. Then, the coordinate of the n^{th} element of the array can be denoted as (r, ϕ_n). Now by applying the same phase correction concept for the array placed on a wedge, the amount of required phase compensation can be computed as

$$\Delta\phi_n^c = +kr|\sin(\phi_n) - \sin(\phi_{n-1})| \tag{2.19}$$

Again, the expression in (2.19) assumes a scan angle of $\phi_s = \pi/2$.

CHAPTER 3. PHASED ARRAY ANTENNA TEST PLATFORM

3.1. Introduction

This chapter presents the details involved with the phased array antenna test platform.

3.2. Motivation for Work

The function of an antenna array depends on two individual parameters in terms of the operating signal, amplitude and phase. By controlling these two parameters on each individual element of the array, different types of spatial distributions of the radiation pattern and beam scanning methodology can be achieved. In particular, controlling the phase of the signal on each element gives the characteristics of beam steering to reconstruct the radiation pattern for optimum functionality. These attributes of the antenna array can be very useful for designing a conformal type array antenna. When the surface of the conformal array changes its shape, the spatial orientation of the antenna changes resulting in a deformation of the radiation pattern of the array. To recover the desired radiation pattern in a particular direction, the amplitude and phase of the signal received by each individual element need to be selectively controlled. One way to do this is to process the signals received by each individual element prior to being analyzed. The processing method of received signals can be done by exploiting small signal processing units or by designing RF circuitry consisting of voltage variable attenuators and voltage controlled phase shifters. Although these components are available commercially, the difficulty here will be the complexity due to the integration of all these components in a proper way to control the behavior of the integrated RF circuit in the desired manner.

3.3. Description of Work

The antenna array under test along with the designed RF circuit will be denoted as the phased array antenna test platform in this discussion. The test platform has been designed to be compatible with any conformal antenna array and consists of four individual elements working at 2.45 GHz. This work will validate the phase compensation expression evaluated in the previous chapter for the practical implementation of the phase compensation circuitry for the conformal array antenna. The test platform has been designed to work as a receiver and consists of several blocks, as shown in Fig. 14. The schematic of the RF test platform is depicted in Fig. 15 where the symbols G, dB, $\Delta\Phi$ and Σ refer to amplifier, attenuator, phase shifter and power combiner, respectively. The details for each block are discussed on following sections.

Figure 14. Block diagram of the proposed system.

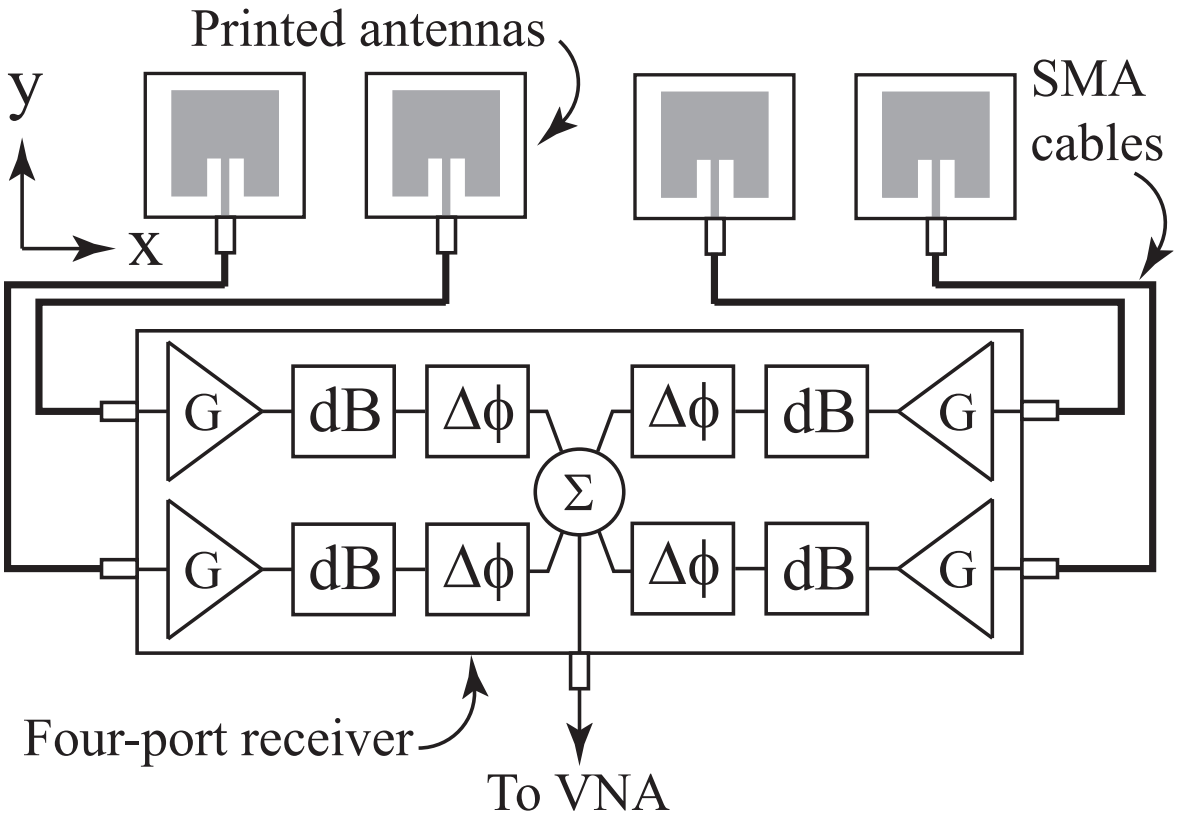

Figure 15. Schematic of the antenna test platform.

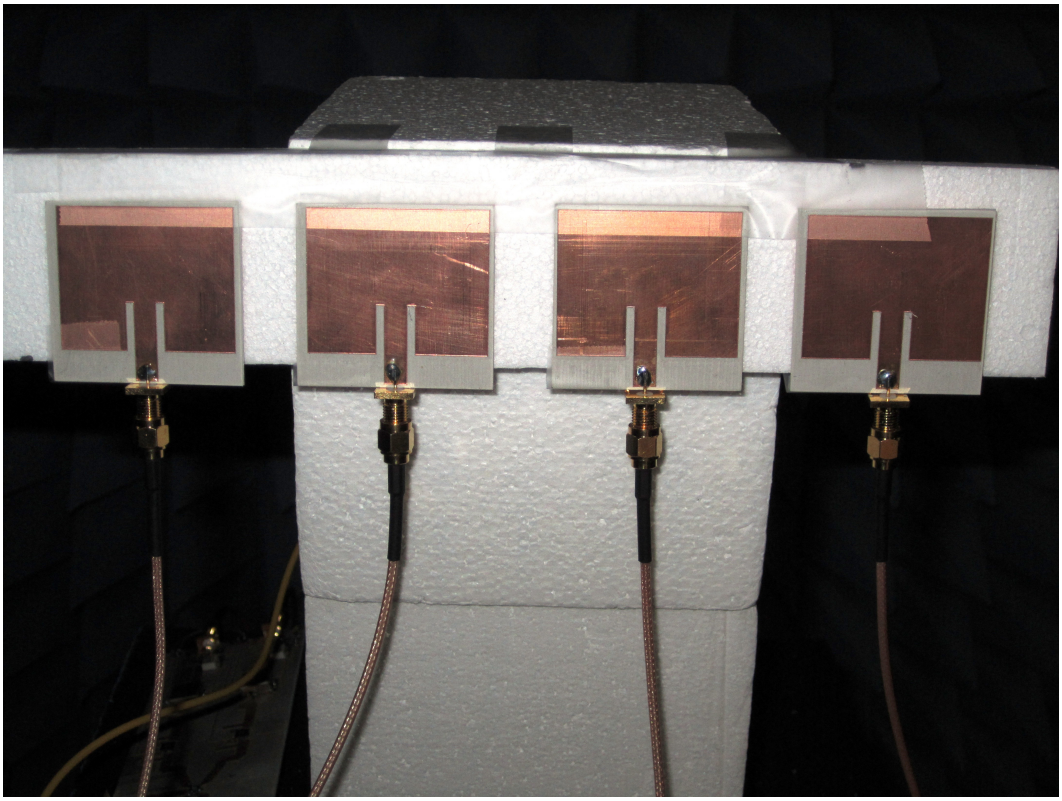

Figure 16. Four individual microstrip patch antennas on a non-conducting surface.

3.3.1. Four element Antenna Array

Four identical individual microstrip patch antennas working at 2.45 GHz have been designed and printed as a part of the test platform. These four antennas can be realized as an array. These patches, as shown in Fig. 17(b), were manufactured on a 60 mil thick Rogers RT/duroid 6002 substrate ($\epsilon_r = 2.94, \tan\delta = 0.0012$, where ϵ_r is the relative permittivity and $\tan\delta$ is the lost tangent of the substrate) and placed on a non-conducting Styrofoam surface with $\lambda/2$ spacing, as shown in Fig. 16. These patches, as shown in Fig. 18 can be attached to any wedge of a certain angle or to a circular surface of any radius.

3.3.2. Coaxial Cable to SMA Connectors

Four individual patch antennas have been connected to the RF circuit board by four identical coaxial to SMA *(SubMiniature version A)* connectors. Being equal in length and identical in nature, all of these connectors offer equal path delay of the signal to the patches resulting in a zero path delay of the signal between four patches with respect to the each other.

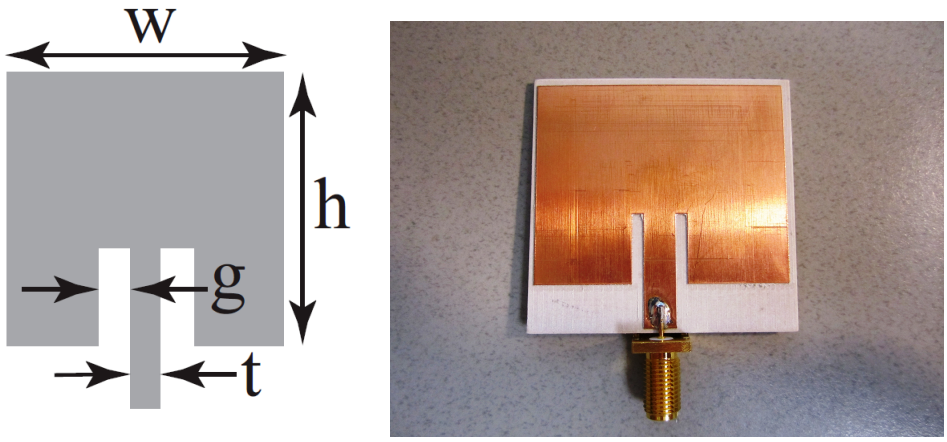

(a) (b)

Figure 17. a) Printed individual microstrip patch antenna with detail geometry (g = 2.0 mm, h = 35.6 mm, t = 5.5 mm, w = 43.6 mm) and b) the fabricated prototype

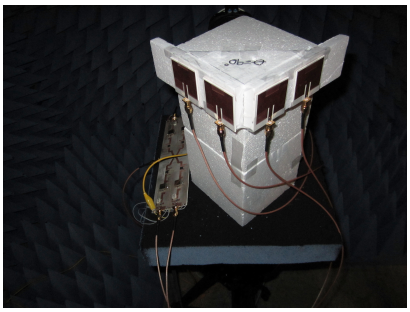

(a) Arrays made of individual patches on wedge-shaped surface.

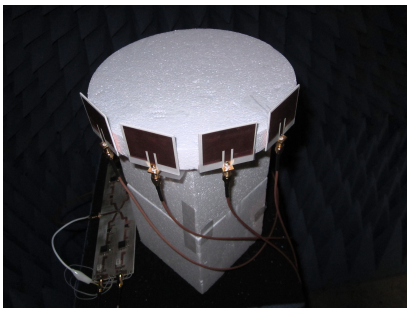

(b) Arrays made of individual patches on singly curved circular shaped surface.

Figure 18. Conformal array made of individual microstrip patches.

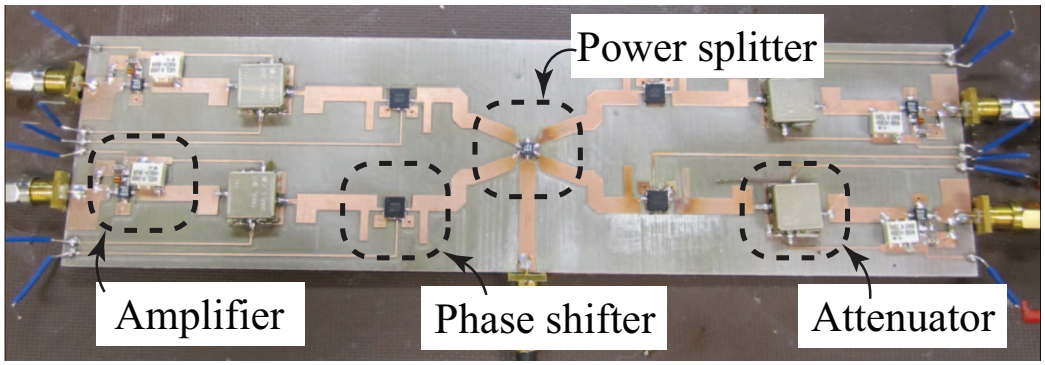

Figure 19. Picture of the four port receiver.

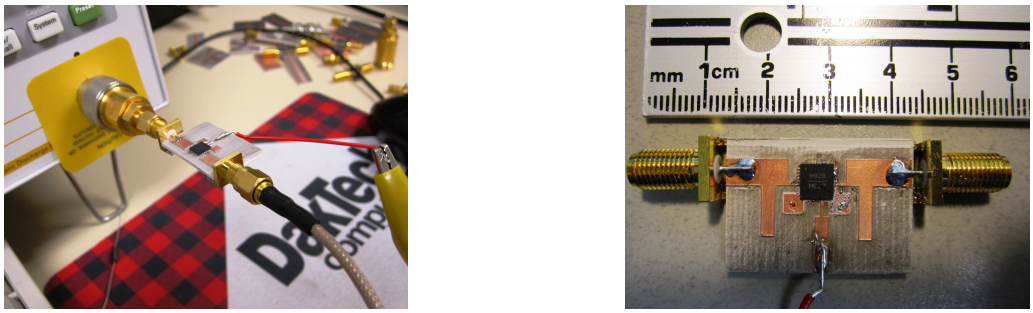

Figure 20. Voltage Controlled Phase Shifter under test.

3.3.3. Four-Port Receiver RF Circuit Board

The four-port receiver RF circuit board is a MISO *(Multiple Input Single Output)* system with four input ports and one output port, as shown in Fig. 19. This board was developed on a 60-mil thick Rogers RT/duroid 6002 substrate $(\epsilon_r = 2.94, \tan\delta = 0.0012)$ to be operated at 2.45 GHz and consists of several individual blocks such as power amplifier, voltage-controlled phase shifter, voltage variable attenuator, amplifier and microstrip transmission line.

The voltage-controlled phase shifters used in the board are manufactured by Hittite Microwave Corporation (part number: HMC928LP5E) [42]. These analog phase shifters can offer a range of $0\,^\circ$ to $450\,^\circ$ normalized phase shift for a 0 V-13 V control voltage. The pictures in Fig. 20 were taken during the S-parameter measurements of an individual phase shifter at 2.45 GHz. The phase shifter is being tested on the same substrate as the RF board. As Fig. 21 suggests, the measured reflection coefficient, S_{11}, has a 10-dB cutoff at 2.45 GHz. The measured magnitude and normalized phase of the tranmission

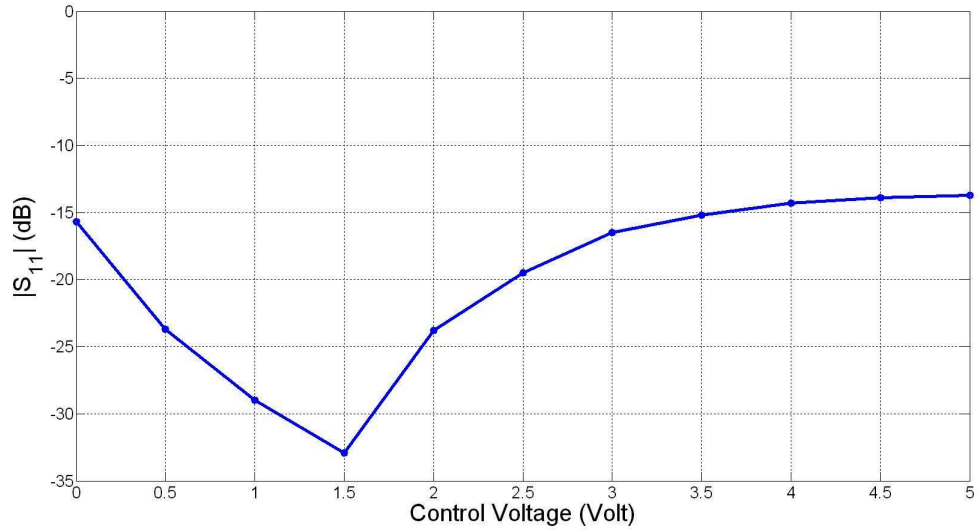

Figure 21. S_{11} of the phase shifter at 2.45 GHz.

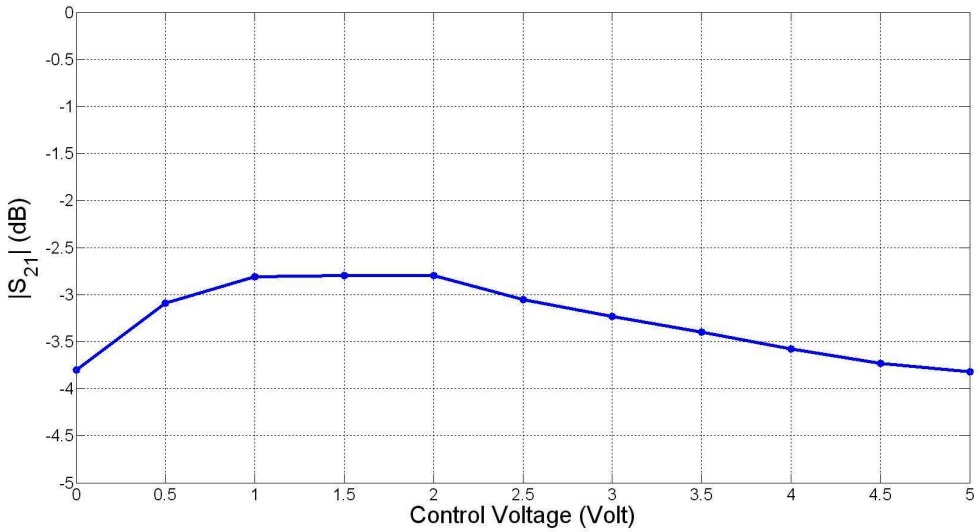

Figure 22. Magnitude of S_{21} of the phase shifter at 2.45 GHz.

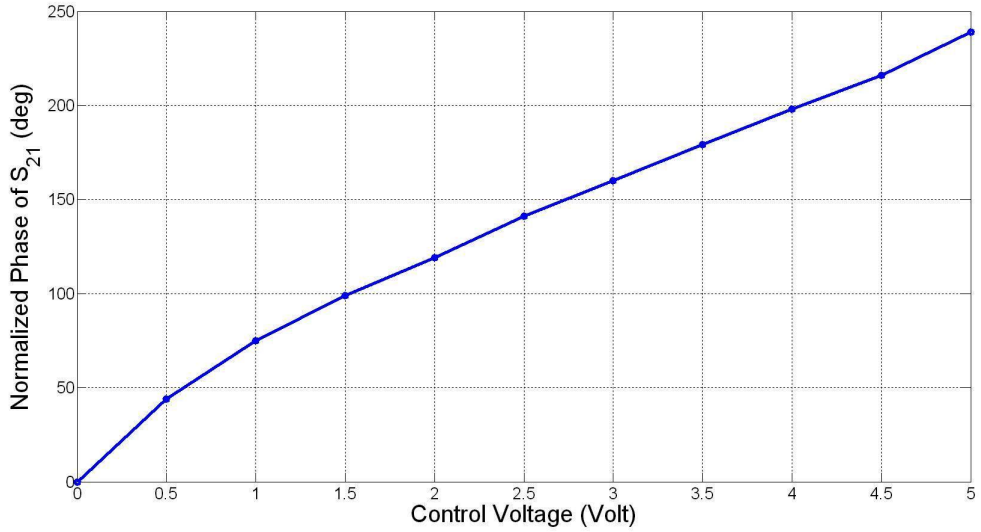

Figure 23. Normalized Phase of S_{21} of the phase shifter at 2.45 GHz.

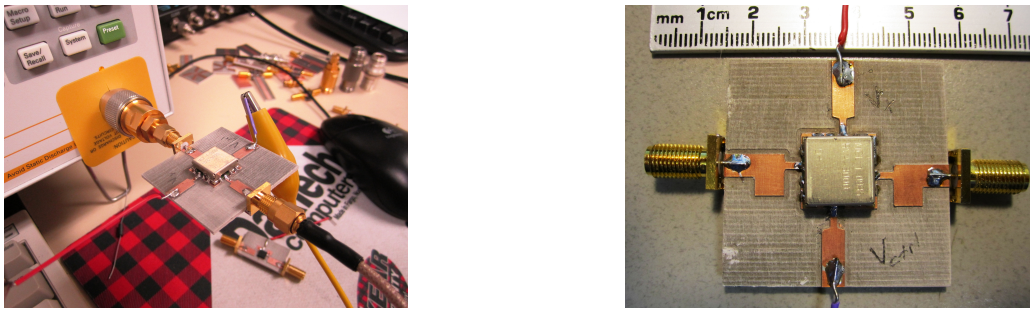

Figure 24. Voltage Variable Attenuator under test.

coefficients S_{21} are shown in Figures 22 and 23, respectively. For all of the cases, the control voltage has been varied from 0 V to 5 V, as plotted along the $x-$axis because of the fact that the normalized phase offered by the phase shifter for such span of control voltages would be enough for the scope of this current work. The four individual phase shifters controlled by four different control voltages have been implemented to control the phases of the signals received from each individual four patches separately. These control voltages can be operated through the LabVIEW graphical user interface (GUI) (which will be discussed later).

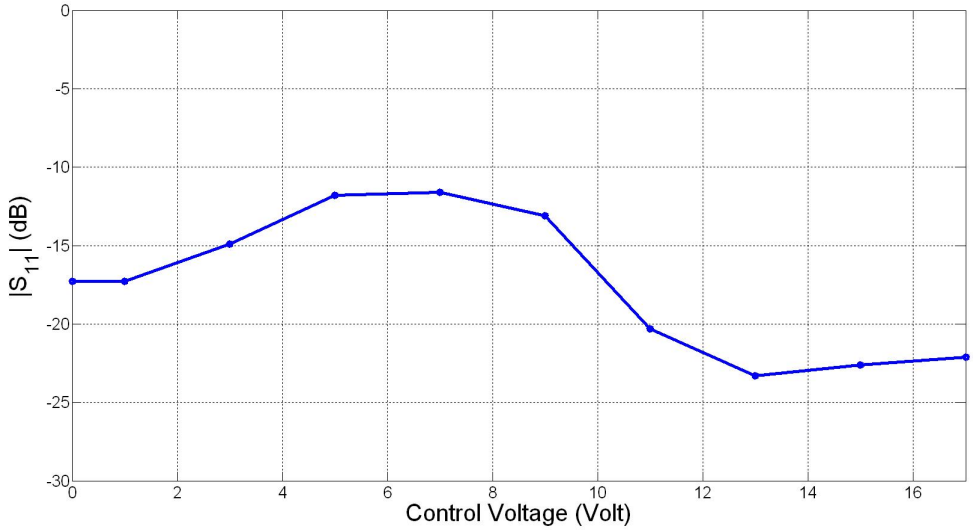

Figure 25. $|S_{11}|$ of the Attenuator at 2.45 GHz.

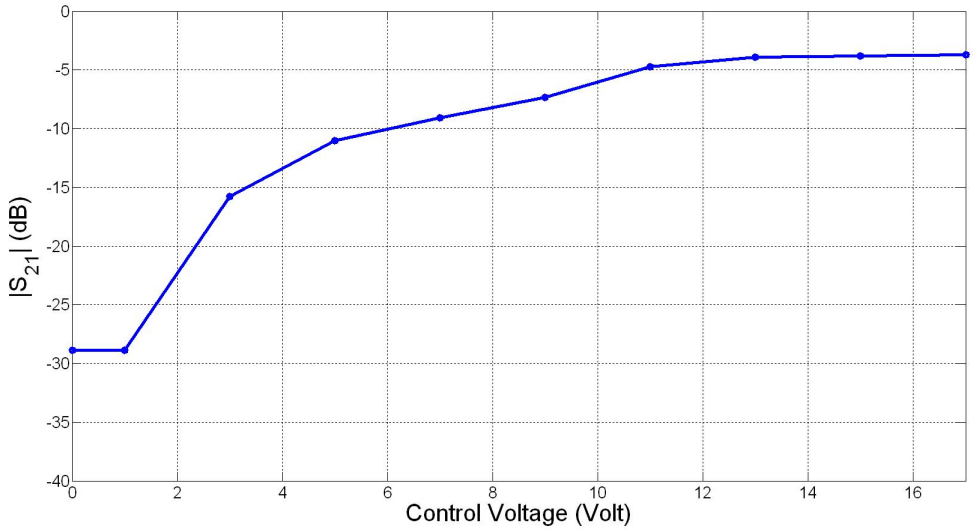

Figure 26. Magnitude of S_{21} of the Attenuator at 2.45 GHz.

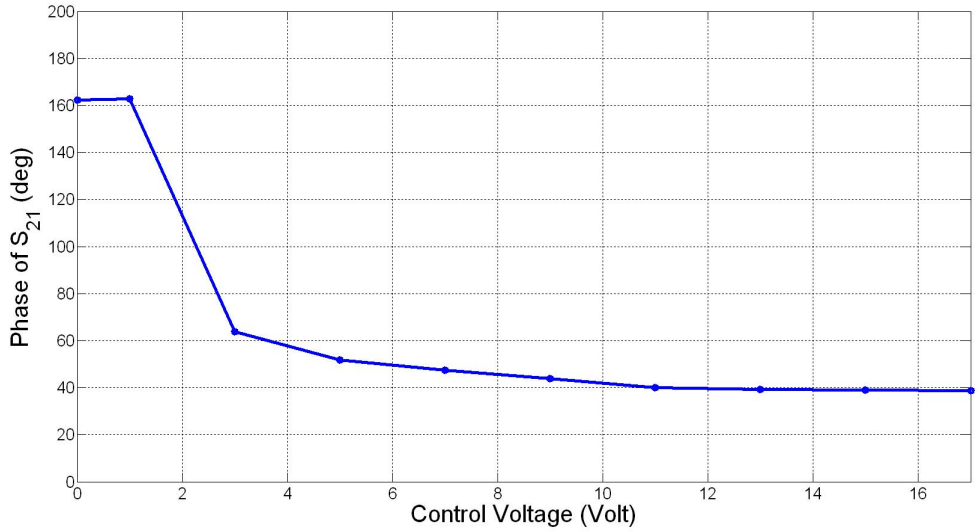

Figure 27. Phase of S_{21} of the Attenuator at 2.45 GHz.

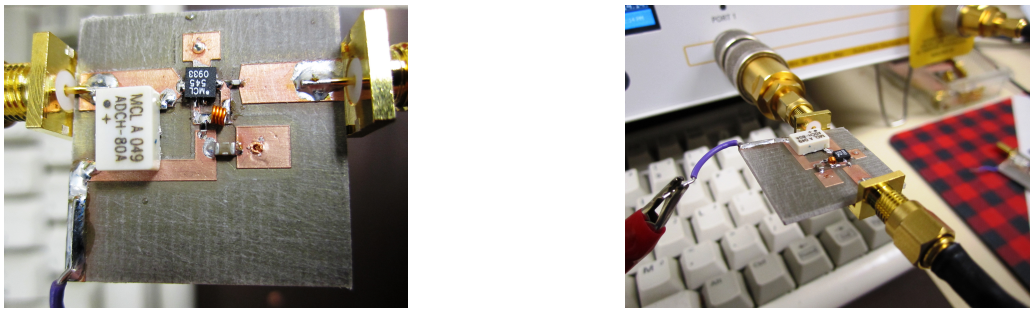

Figure 28. Low Noise Amplifier under test.

The voltage variable attenuators used in the RF board are manufactured by Mini-Circuits (part number: RVA - 3000+) [41]. These attenuators can offer attenuation in a range of 4 - 45 dB for input control voltages of 18 V - 1 V. The pictures in Fig. 24 have been taken during the S-parameter measurements of an individual attenuator at 2.45 GHz. The results in Fig. 25 show that the measured reflection coefficient S_{11} has a good 10 dB cutoff at 2.45 GHz. The measured magnitude and phase of the tranmission coefficients S_{21} are also shown in Figures 26 and 27, respectively. These attenuators are connected in series with the phase shifters through a microstrip transmission line for achieving amplitude variation of the signals received from the patch antennas and can be controlled by the LabVIEW GUI.

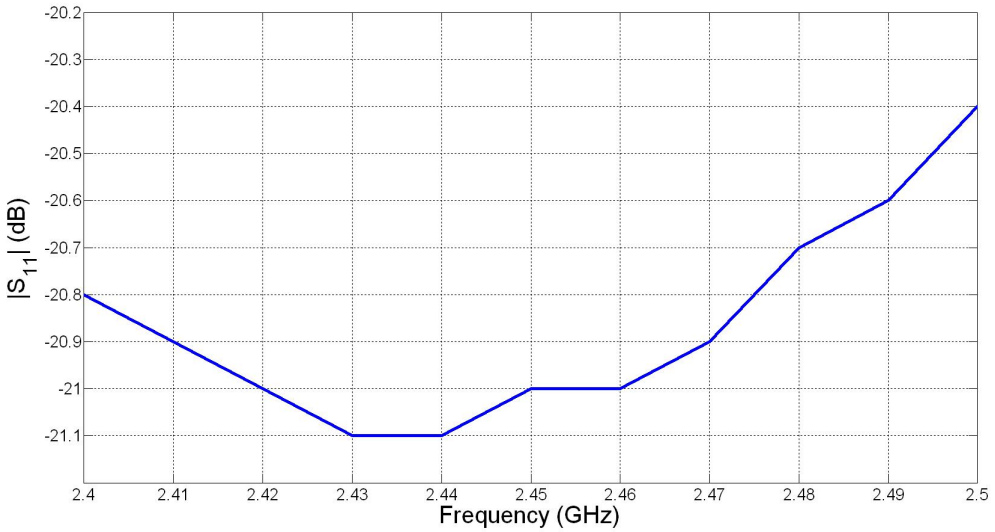

Figure 29. $|S_{11}|$ in dB of the Amplifier from 2.4 to 2.6 GHz.

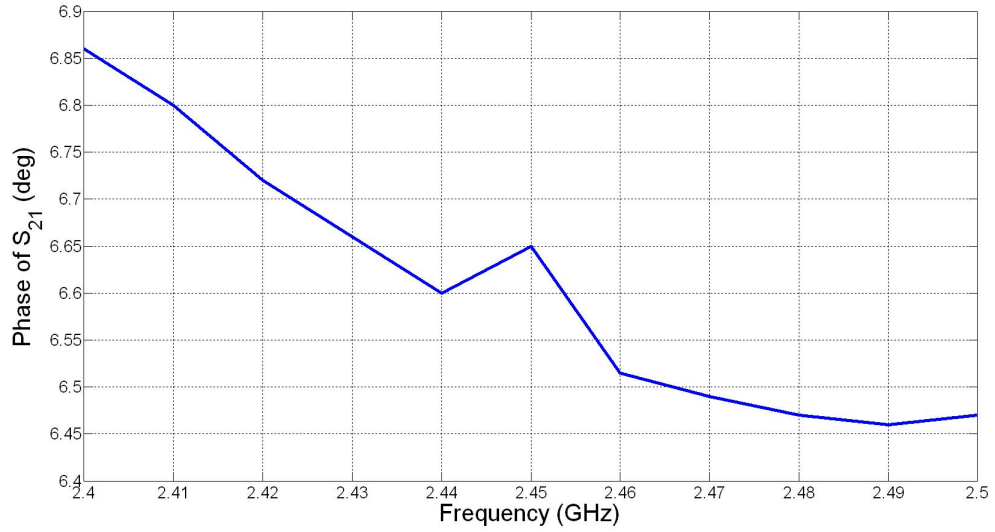

Figure 30. Phase of S_{21} of the Amplifier from 2.4 to 2.6 GHz.

The low noise amplifiers (LNA) used in the RF board are manufactured by Mini Circuits (part number: PMA 545+) [41]. These amplifiers have been used to enhance the level of the received signals from the patches to compensate for the insertion loss of the phase shifters and attenuators. A multiline inductor manufactured by (part number: MCL A049 ADCH - 80A) Sunlord [47] has been integrated along with the LNA for achieving a stable amplification. The pictures in Fig. 28 were taken during the S-parameter measurements of an individual amplifier at 2.45 GHz. The results in Figures 29 and 30 show the measured reflection coefficient S_{11} and magnitude of transmission coefficients for a span from 2.4 GHz to 2.6 GHz, respectively. The limitation of the amplifier can be seen from the step-like response with respect to the network analyzer. However this limitation can be ignored for this project as the responses at 2.45 GHz will be the points of interest .

The signals were combined by the power combiner (part number: WP4R+) manufactured by Mini-Circuits [41]. The combined signal from the power combiner was then sent to the network analyzer for analyzing the overall response of the system as a single unit. The pictures in Fig. 31 have been taken during the S-parameter measurements at 2.45 GHz. Figures 32 and 33 show the measured reflection coefficient S_{11} of the summing port with ports 1 to 4 terminated with 50Ω and port 1 with the other ports terminated with 50Ω from 2.4 GHz to 2.6 GHz, respectively. The phase shifts between the input ports and the output port have been measured to be $\Delta\Phi_{1C} = -161\,^{\circ}$, $\Delta\Phi_{2C} = -170\,^{\circ}$, $\Delta\Phi_{3C} = -171\,^{\circ}$ and $\Delta\Phi_{4C} = -152\,^{\circ}$.

3.3.4. DAC Controller Circuit

The Texas Instruments DAC 7718 [48] is a 12 bit, octal, 64-pin, low power digital to analog converter (DAC) that takes digital serial data as input and generates analog outputs in eight different channels ranged from either $\pm$2 V to $\pm$16.5 V in bipolar operation or 0 V to +33 V in unipolar operation. The state of the operation of the chip depends upon the analog power supply, based on which it acts in bipolar state while connected to a $\pm$15.5-V supply or in unipolar state while connected to a +30.5-V power supply. However, as the RF test platform in this case is designed to be worked only in the range from 0 V to 15 V, a +15-V power supply (V1) has been used as the analog power source of the chip and all the necessary parameters of the DAC have been set to the designated values as provided in the datasheet to be operated in the unipolar state. The connection setup of the entire system can be seen in Fig. 34. From the perspective of digital operation, the DAC accepts inputs in the range from 0.3 Volt to 0.8 Volt as lowlevel input and 3.8 Volt to 5.3 Volt as highlevel input. +5 Volt digital power supply for the DAC system has been achieved by designing a voltage limiter circuitry that takes +15 Volt analog power supply as the input and produces a constant +5 Volt at the output. National Semiconductor

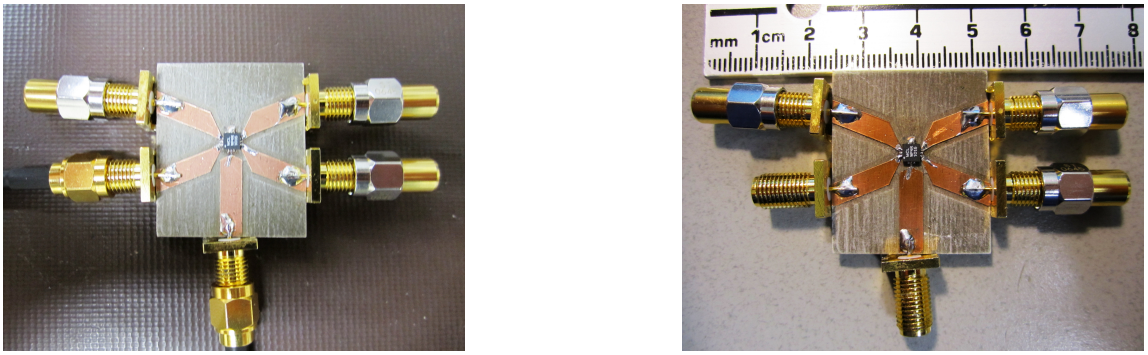

Figure 31. Power Combiner under test.

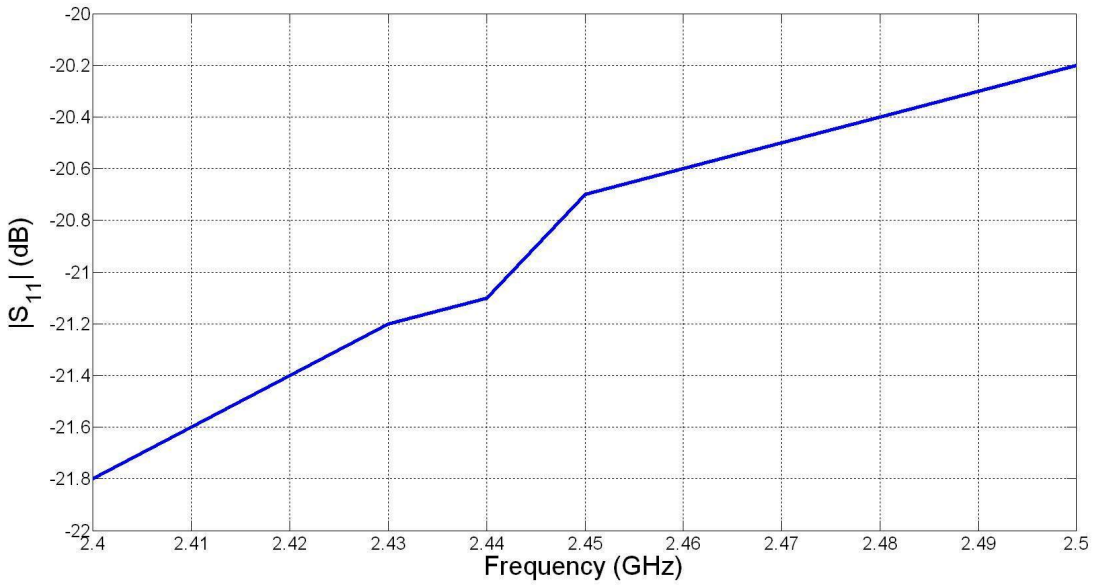

Figure 32. $|S_{11}|$ of the Combiner at Combiner Side from 2.4 to 2.6 GHz.

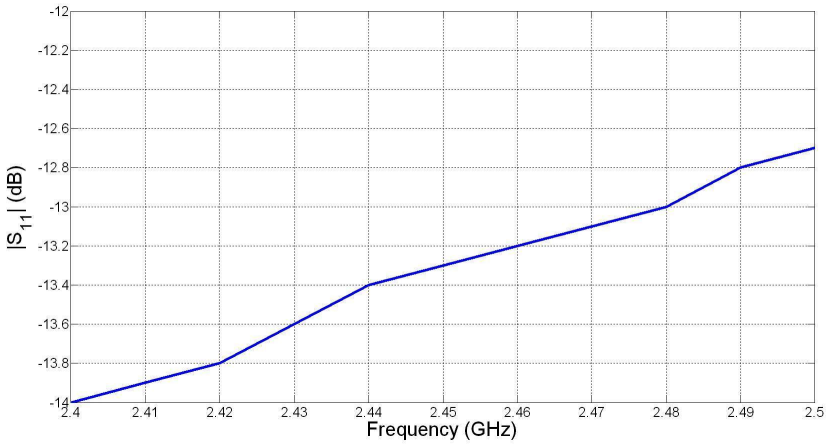

Figure 33. $|S_{11}|$ of the Combiner at one of the branch from 2.4 to 2.6 GHz.

LM78M05 [49], which is a 3−terminal positive voltage regulator offers constant +5 Volt output with the input ranges from +8 Volt to +18 Volt, has been used for this operation. It also offers over voltage protection of the device. As the analog input source is allowed to be a maximum of +15 Volt, therefore the digital input can only have a +5 Volt maximum as the digital source of the chip. Since both the analog source and digital source share a common ground reference, therefore in the RF system analog grounds (AGND) and digital grounds (DGND) refer to the same common ground. The DAC allows for programmable gains of $V_{ref} \times 4$ or $V_{ref} \times 6$ at the outputs where V_{ref} refers to the applied reference voltages that can range from 0 Volt to +5 Volt. The eight analog output channels are divided into two groups, Group A and Group B. Two different reference voltages can be fed separately to them. Thus two different ranges of voltages can be achieved in eight channels, of which first four channels (Group A) yield outputs of one range and last four channels (Group B) yield outputs of another range. In the RF system, Group A channels are connected to the control pins of the analog phase shifters and have to be varied in the range from 0 Volt to +10.5 V, and Group B channels are connected to the control pins of the voltage attenuators and have to be varied in the range from 0 V to +15 V. However, to avoid the circuit complexity and to introduce more application flexibility, the ranges of the outputs in the two groups have been controlled by the interface software in this particular setup rather than by applying separate reference voltages at two groups. Both of these reference voltages of the two groups have been allowed to be connected to a +5 V reference voltage source (V2) so that if needed in the future, any range of outputs between 0 V to +15 V can be achieved by just changing the software parameters and keeping the circuit setup intact.

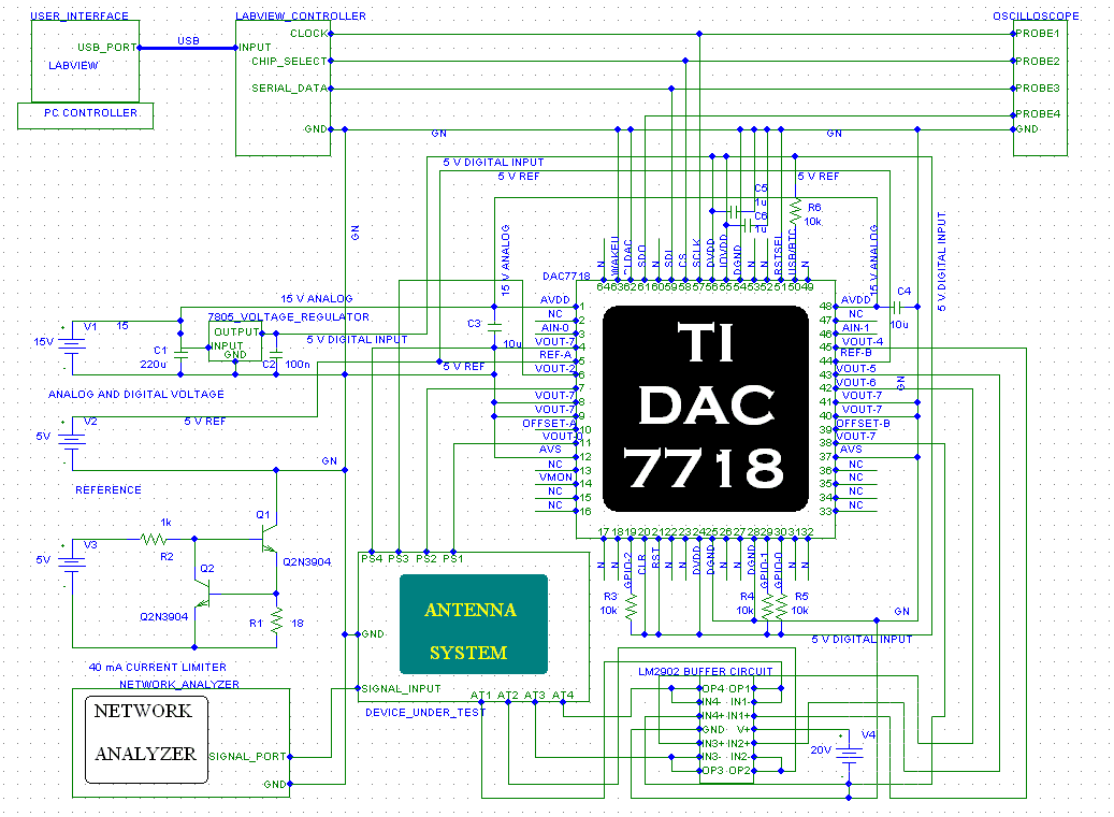

Figure 34. DAC circuitry in details.

The DAC 7718 features a high speed Serial Peripheral Interface (SPI) that can be operated at 50 MHz and is logic compatible at 1.8 V, 3 V or 5 V. All the input data is double buffered. An inverted asynchronous load input (LDAC) transfers data from the DAC data register to the DAC latch and an inverted asynchronous clear input (CLR) sets the output of all eight DACs to AGND. In the SPI Shift Register, the serial data input (SDI) has to be loaded in the device MSB first as a 24-bit word under the control of a serial clock input (SCLK). The register consists of a read/write bit, five register address bits, and twelve data bits. Other bits are reserved for future devices. The falling edge of chip selects (CS) starts the communication cycle. The data is latched into the SPI Shift Register on the falling edge of SCLK while CS is low. When CS goes high, the SCLK and SDI signals become blocked and the serial data output (SDO) pin remains in the high-impedance state. The contents of the SPI shifter register are decoded and transferred to the proper internal registers on the rising edge of CS. The timing for this operation is described in details in the datasheet of the DAC 7718. It offers a maximum settling time of 15sec and a slew rate of 6sec. It can be operated in both asynchronous and synchronous modes.The

resolution of the DAC is 12 bits with a relative accuracy of 1 LSB maximum. For the output in the range of 0 V to +15 V, a resolution of 3.66 mV can be achieved. However for the ease of usage, a precision of 300 mV that meets the criteria of the minimum precision of the analog phase shifters and voltage attenuators of the RF system has been offered in the user interface.

The chip comes in two different packages, Quad Flat No leads (QFN)-48 $(7 \times 7mm)$ and Thin Quad Flat Pack (TQFP)-64 $(10 \times 10mm)$. The TQFP-64 package has been used throughout the testing. SchmartBoard, Inc. TQFP interface [50] has been used to make the circuit connection to the chip. As a low power device, the DAC system can handle only upto $\pm$5mA of current while in operation. For a higher current-rating load, buffer circuits at the outputs is recommended for the protection of the device from burn out. A current limiter circuit that limits the current from the input has been designed to protect the DAC system. This circuit limits the current to about 50 mA. One 5 V voltage source (V3) and two National Semiconductor 2N3904 transistors (Q1 and Q2) have been used to design the circuit. It will act like a normal switch as long as the system draws current no more than 50mA. When the system exceeds beyond such conditions, the circuit will bypass the current to Ground until the current through the system stables back to 50 mA. Resistor R1 (18 Ω) is used as a current sense resistor that monitors the current flowing through the Q1 transistor. The voltage drop across R1 starts to increase as the current through Q1 increases. If the voltage at the top of R1 reaches 0.7 V, Q2 begins to turn on diverting some of the current from the base of Q1 and bypassing the over-rated current to the ground. Thus the whole mechanism protects the system from over-current damage.

3.3.5. LabVIEW GUI

National Instrument LabVIEW 2010 [43] has been used to design a Graphical User Interface (GUI) that offers the user to control the eight output channels of the DAC separately. The GUI basically consists of several logic and functional blocks in its background that controls the DAC through a National Instrument LabVIEW USB 6008 peripheral device. The GUI takes the inputs from the user in analog format and then converts it into desired digital expressions for further processing which produce the desired 24 bit serial digital bit stream to feed it as the SDI signal to the DAC through the Universal Serial Bus (USB) peripheral interface. The peripheral device needs to be connected to the USB port of the system at one end. The other end consists of a total 16 analog and 16 digital ports of which only four digital output ports are used to generate the signals SCLK, CS, SDI and ground reference which are fed to the DAC circuit directly. A four channel oscilloscope can be used to view the SCLK, CS, SDI and SDO signals separately to get the timing information of the DAC circuitry. Overall, this setup presents the user an interactive interface to control each of the devices of the RF system in a very effective way.

Figure 35. a) Picture of the 1 x 4 antenna test platform attached to a non-conducting wedge; b) picture of the 1 x 4 antenna test platform attached to a non-conducting cylinder.

3.4. S-Parameter Measurements and Scanning Properties

The measurement of the Phased Antenna Array Test Platform has been carried out in a fully anechoic chamber. To verify the scanning capability of the conformal array, the scanning characteristics of the test platform have been analyzed. At first, the antennas were attached to a flat surface and the S-parameters and radiation pattern have been measured. The picture of the test setup is shown in Fig. 35 a). The measured return loss is shown in Fig. 36 and the scanning characteristics measured in the chamber are shown in Fig. 37. For comparison, the analytically computed array patterns for a uniformly excited, equally spaced linear array (UE, ESLA) [14] has been shown also. Good comparison has been observed between the predicted and measured results which validate the fact that all of the RF blocks in the four port receiver are operating correctly, especially the phase shifter. For all of the cases, the interelement spacing was kept fixed at a value of $\lambda/2$.

3.5. Phase Compensation and Pattern Correction Results

When the array was attached to the non-conducting wedge shaped surface shown in Fig. 35 a) and the non-conducting cylindrical surface shown in Fig. 35 b), the phase compensation expressions in equation (2.18) and equation (2.19) can be implemented to correct the behavior of the array. This can be done by careful adjustment of the control voltages of individual phase shifters which offer exact phase compensation to each array element with respect to the analytically computed phase compensation values.

3.5.1. Analytical Work for Correction of Field Pattern of The Test Platform

The expression of Array Factor (AF) has been described as equation (2.8) in chapter 2 for Cartesian coordinate system. For analytical computations, the same parameter can be redefined in a Spherical

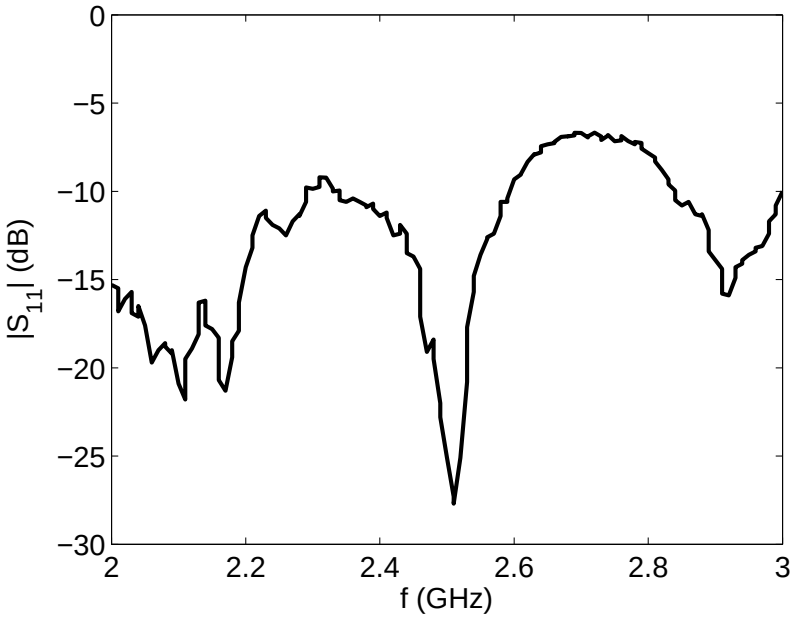

Figure 36. Measured S_{11} of the 1 x 4 antenna test platform.

coordinate system as,

$$AF = \sum_{n=1}^{N} w_n e^{jk[x_n(u-u_s)+y_n(v-v_s)+z_n\cos\theta]} \tag{3.1}$$

Equation (3.1) assumes $u = \sin\theta\cos\phi$, $u_s = \sin\theta_s\cos\phi_s$, $v = \sin\theta\sin\phi$, $v_s = \sin\theta_s\sin\phi_s$, θ_s is the elevation steering angle, ϕ_s is the azimuth steering angle and w_n is the complex weighting function. For this work, an element factor of $e(\theta) = A\cos\theta$ was defined and each complex weighting function was defined as $w_n = e(\theta)e^{j\alpha}$ where α was the voltage angle used to scan the array and the attenuator was used to control the amplitude A of each element. Then to analytically compute the compensated radiation pattern and validate the measurements of the test platform on a conformal surface, the following compensated Array Factor (AF_c) was used:

$$AF_c = AFe^{j\Delta\phi_n} \tag{3.2}$$

3.5.2. Phase Compensation Results

The measurement of the radiation pattern of the test platform with phase correction has been carried out next. To do that, the antenna test platform has been attached to the wedge shaped conformal surface, as shown in Fig. 35 a) with bend angles $\theta_b = 30^\circ$ and 45° with an element spacing of $\lambda/2$.

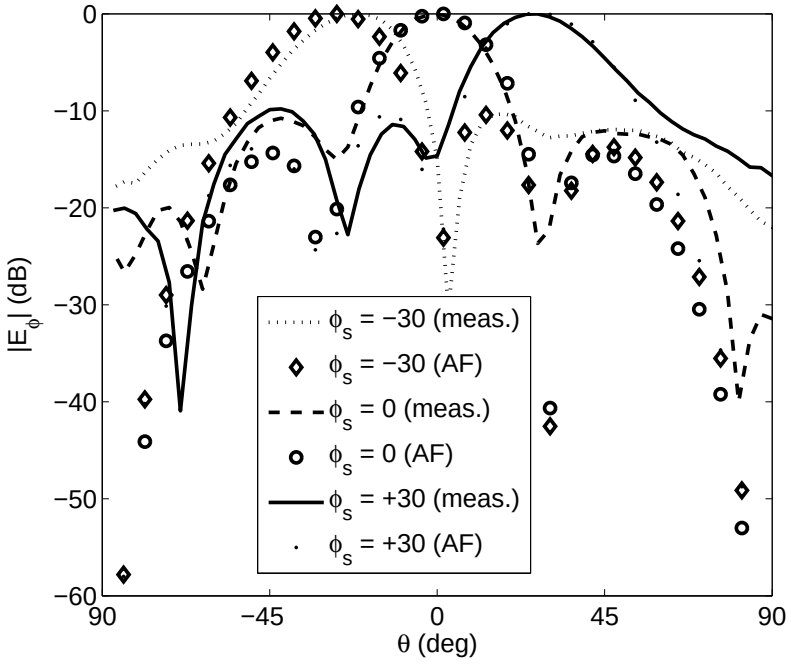

Figure 37. Measured and analytical scanned patterns in the $x-z$ plane for the 1 x 4 antenna test platform on a flat surface ($\theta_b = 0^\circ$).

The radiation pattern was then measured at 2.45 GHz in $x-z$ plane for both the compensated and uncompensated cases. Figures 38 and 39 show the pattern correction results for $\theta_b = 30^\circ$ and 45°, respectively. The uncorrected radiation pattern was measured at first when the surface of the array was changed to a non-planar orientation but the control voltages to all of the phase shifters were set to equal value (no phase compensation). Next, the control voltages of the phase shifters were changed carefully to achieve the corrected results. The technique used here is to change the reference plane of the array to a new reference plane where the elements $A_{\pm 1}$ are lying, as shown in Fig. 12. By defining this new plane as the reference, only the voltage of the phase shifters feeding elements $A_{\pm 2}$ have to be changed to adjust the radiation pattern. The antenna factor terms in equation (3.1) and equation (3.2) were used next to analytically compute the pattern of the array on both wedge-shaped conformal surfaces. In particular, the uncorrected antenna patterns were computed using equation (3.1) and these results are shown in Figures 38 and 39 and the corrected antenna patterns were computed using equation (3.2) and these results are also shown in Figures 38 and 39. Next, the performance of the antenna test platform was carried out on a cylindrical surface with radius 10 cm. The interelement spacing of the array was kept $\lambda/2$ and the measurement was taken at 2.45 GHz. The test setup can be seen in Fig. 18(b). The

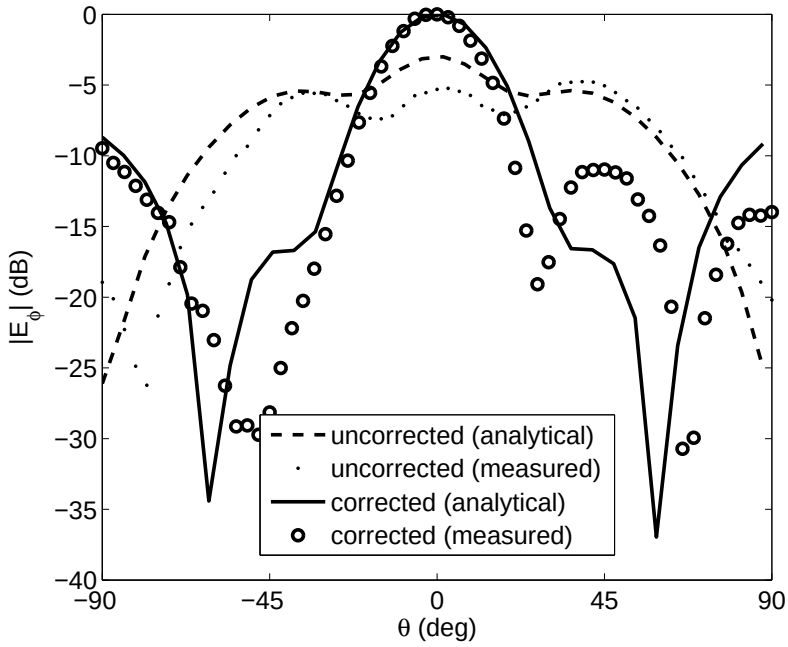

Figure 38. Measured and analytical patterns at 2.45 GHz in the x-z plane for the 1 x 4 antenna test platform on a wedge with $\theta_b = 30^\circ$.

required phase compensation was calculated using equation (2.19) and has been presented in Fig. 40. In all cases, good agreement between the measurements and the analytical computations can be observed. A small amount of asymmetries can be seen in all of the measured field patterns with respect to $\theta = 0^\circ$ which can be explained as the measurement error due to limitation of the measurement equipments and the small anechoic chamber.

3.6. Gain Calculation and Compensation Results

Gain of an antenna system to a particular direction can be defined by the total accepted power normalized by the corresponding isotropic intensity at that direction for the antenna. On the other hand, directivity of an antenna system towards a particular direction can be defined by the radiation intensity normalized by the corresponding isotropic intensity at that direction for the antenna. Theoretically if there is no loss due to the mutual coupling in the antenna system, the gain and the directivity will be the same. The mathematical relation between gain (G) and directivity (D) can be expressed as

$$G = eD \tag{3.3}$$

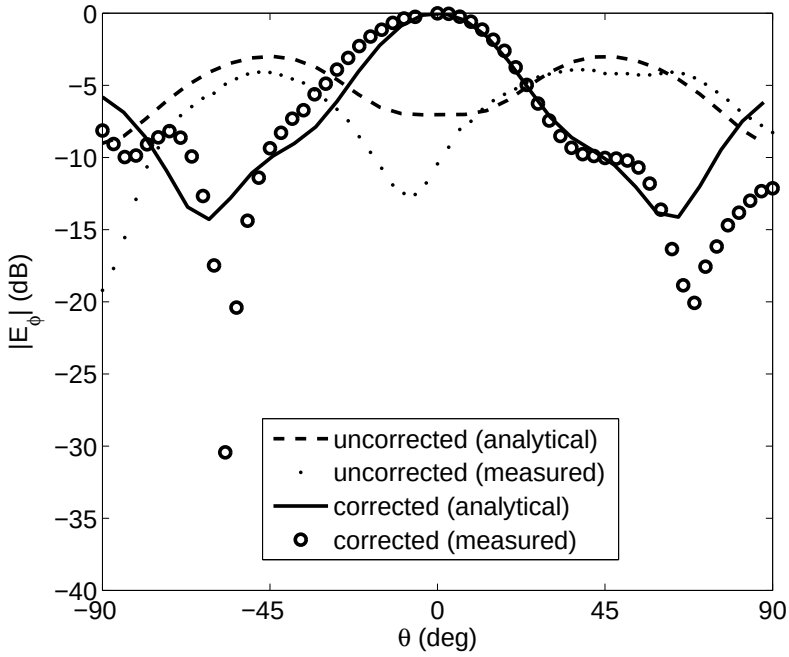

Figure 39. Measured and analytical patterns at 2.45 GHz in the x-z plane for the 1 x 4 antenna test platform on a wedge with $\theta_b = 45^\circ$.

The term e in the equation (3.3) is known as the efficiency of the antenna system which may be defined as the ratio of the total power radiated by the antenna to the net power accepted by the antenna from the connected transmitter for an antenna system. Practically the gain of an antenna can never be equal to the directivity of that antenna as the gain depends also on the efficiency of the system. But to analyze the gain of a system, the analysis of directivity is required. So it can be said that if the efficiency of an antenna system does not change, the change in the directivity by a factor will lead to an equivalent change in the gain of the system by the same factor.

The above concept can be used also to analyze the gain of the array system described in this work. The directivity of an array can be found using the array factor equation [6],

$$D = \frac{4\pi |AF_{max}|^2}{\int_0^{2\pi}\int_0^{\pi} |AF|^2 \sin\theta \, \mathrm{d}\theta \mathrm{d}\phi} \tag{3.4}$$

A uniform linear array of N number of elements with constant element spacing of *d* along the $z-$axis is symmetric with respect to ϕ and therefore the directivity of the array can be numerically computed and

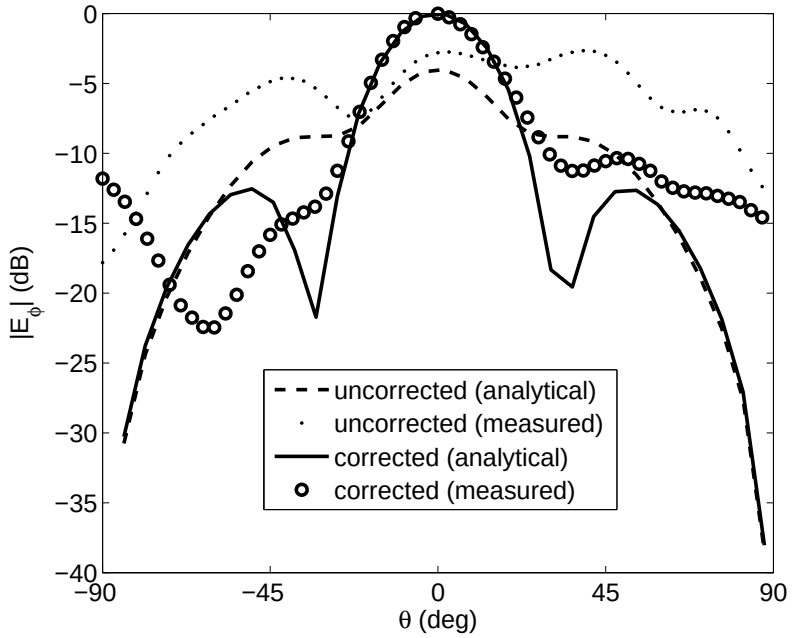

Figure 40. Measured and analytical patterns at 2.45 GHz in the x-z plane for the 1 x 4 antenna test platform on a cylinder with a radius of curvature of 10cm.

expressed as

$$D = \frac{N^2}{N + 2\sum_{n=1}^{N-1}(N-n)\,\mathrm{sinc}(nkd)\cos(nkd\cos\theta_s)} \tag{3.5}$$

For the element spacing of $d = 0.5\lambda$, equation (3.5) simplifies to,

$$D \simeq N \tag{3.6}$$

For the element spacing up to a wavelength, the directivity increases almost in a linear fashion [2]. But as the element spacing increases further, the denominator in equation (3.5) also increases while the maximum value of AF in the numerator remains same. This results to a decrease in directivity of the array. Moreover, as the element spacing exceeds a wavelength, appearance of grating lobes results a sharp drop in directivity [6]. The decrease in directivity due to the grating lobe becomes more dramatic as the number of elements increases, because the main beam and grating lobes have narrower bandwidths which results in to a large change in AF for a small change in θ [2].

Refer to Fig. 12, when the surface of the array was bent in a certain angle, the phase shifter has been used to correct the radiation pattern. This has been done by adjusting the reference plane of the

antenna. Although the array elements can be realized to be belonged virtually on a same plane by this phase compensation technique but a change in inter-element spacing can be noticed through this process. When the array element A_{+2} has been projected on the plane where A_{+1} was lying, the effective spacing between A_{+1} and projected A_{+2} got reduced by a factor of $(1 - \sin\theta_b)$. Now, as the default spacing was 0.5λ, therefore any further reduction of spacing would be result in a reduced directivity.

When the conformal array changes its shape, the associated gain of the overall array also changes therefore. The reference gain $G_r(\theta, \phi)$ of the array can be defined as the gain of the array in a certain direction when the antenna array is attached to a particular surface. Now as the surface changes, the associated field pattern of the array also changes. To compensate this change, when the phase correction method is applied to the array system, the shift in the gain of the antenna has been observed. If this new compensated gain of the array system is denoted as $G_c(\theta, \phi)$ and the shift in gain is described as $G_s(\theta, \phi)$ then the relationship between them can be expresses as:

$$G_s(\theta, \phi) = G_c(\theta, \phi) - G_r(\theta, \phi). \tag{3.7}$$

This computed gain shift value can then be compared to measurements to determine if the antenna pattern is recovered or corrected. As mentioned before, the gain broadside to the antenna will be measured and the reference surface used to evaluate $G_r(\theta, \phi)$ is assumed to be flat ($\theta_b = 0^\circ$).

Table 1. Gain Shift Values for the Antenna Test Platform.

Surface	$G_{s,analy.}$	$G_{s,meas.}$	Proj. spacing
$\theta_b = 30^\circ$	-0.6 dBi	-1.0 dBi	0.43λ
$\theta_b = 45^\circ$	-1.3 dBi	-1.8 dBi	0.35λ
Cylinder	-0.8 dBi	-1.6 dBi	non-uniform

The measured and computed gain shift values are also shown in Table 1 for all three test cases (wedge with $\theta_b = 30^\circ, 45^\circ$ and a cylinder). The analytical values were computed using the gain expressions presented in [6] for a non-uniformly spaced array. Although the radiation pattern can be recovered for an array antenna by technique of projection of plane but the trade-off will be the reduced gain and hence this is the limitation of the proposed technique.

CHAPTER 4. THE FOUR ELEMENT SELFLEX ARRAY DESIGN

4.1. Motivation

The conformal array design presented on previous chapter validates the concept of phase correction theory. However from the perspective of design guidelines, there were several drawbacks in that type of system. First, the array was realized by placing four patch antennas, designed on different substrate surfaces. But in a practical scenario, a microstrip patch antenna array is generally realized on a single substrate. Therefore to be applicable physically, all of the elements of the conformal array need to be designed on the same flexible substrate. Secondly, the associated RF test platform that has been used to correct the functionality of the array was controlled manually. This limitation actually slows down the performance of the array. Therefore, if any methodology can be developed to compensate the phase to the array elements in an autonomous manner, then this limitation can be overcome. Third, the array system designed earlier could not be operated without the RF test platform. Though developing the RF system each time for an array is neither cost effective nor space constrained solution but for validation of the theoretical work, that block was a necessary part of the array system in general. Altogether, the challenges here are to design an autonomous conformal array system prototype which can maintain the same performances like the RF test platform but can offer more compactness, cost-effective, less complex and faster response for practical feasibility.

The new four element SELFLEX (SELF-adapting FLEXible) array design proposed in this chapter not only consists of the array elements designed on a single substrate but also offers autonomous correction of the field pattern during its conformal activity with the help of a simple circuit embedded on the surface of the array. The first challenge was met by designing the four patches with only a single feed network. This has been achieved by exploiting of parallel feed network, described in chapter 1, in the array system. The second challenge, the development of an autonomous correction circuitry has been achieved by introducing a sensor circuit. This feedback network offers the system with necessary phase compensation by sensing the curvature of the antenna by a flexible resistor, attached to the conformal surface of the array. Finally the remaining challenge was met by elimination of the devices that were integrated earlier in the RF test platform. One objective of this project is to meet the specific goal of autonomous correction of the radiation pattern for an array system. To meet this, only the phase of the driving signal on each patch has to be controlled separately. Thus by ignoring the other functional RF blocks, only the phase shifters have been embedded on the substrate of the SELFLEX (SELF-adapting FLEXible) array and the necessity of the RF test platform has been eliminated. The new proposed design is shown in Fig. 42

where the sensor circuit block and small black phase shifters can be seen clearly. However the flexible sensor, which has been attached at the back of the array surface, is not visible here. The elements in the array are designed to operate at 2.47 GHz on a thin and flexible 20 mil Rogers RT/duroid 6002 substrate and have a spacing of $\lambda/2$.

4.2. Description of Work

The design of the four element SELFLEX array is described in this section.

4.2.1. The Resistive Sensing Circuit

In the conformal array design proposed in the previous chapter, the phase correction of the each array element has to be controlled manually. Each time the surface of the array changes, the user has to change the control voltage of the phase shifter through the LabVIEW GUI to provide the array adequate phase compensation. This limitation has been overcome in the new design of SELFLEX array by introducing a sensor circuit that consists of a flexible resistor manufactured by Spectra Symbol [46]. This new feature enables the array to correct its functionality autonomously in time. A schematic of the sensor circuit is shown in Fig. 43. The resistor senses the amount of curvature of the surface of the array each time and feeds that information to an OpAmp circuit. An AMP04 precision single-supply instrumentation amplifier manufactured by Analog Devices [45] has been used in the sensor circuit which provides the necessary control voltage of the phase shifters for various values of θ_b to compensate the field pattern of the array in its non-planar activity. To realize the functionality, a text fixture consisting of the flexible resistor attached to a wedge-shaped conformal surface was constructed. The sensor circuit was then connected to the resistive sensor and the output control voltage V_{ctrl} of the circuit was connected to a prototype board including a single Hittite voltage controlled phase shifter. The text fixture was then used to bend the resistive sensor at various angles of θ_b and the associated phase shift was measured at 2.47 GHz using a network analyzer. The measured and analytical normalized phase shift obtained from the sensor circuit have been shown in Fig. 44. As both results match pretty well, this sensor circuit has been used in the array system along with the Hittite phase shifter to achieve the autonomous phase correction feature for the array.

4.2.2. 1×4 SELFLEX Array Prototype

The 1×4 SELFLEX array introduced in this chapter is a new type of self-adapting conformal array. The self-adapting capability of the array has been achieved by the sensor circuit described in the previous paragraph. In this paragraph, the detail design related to the 1×4 microstrip patch array has been described. In case of the RF test platform, it was shown that the elements of the array were developed using the same substrate but on discrete surfaces. However, such designs are not efficient for practical

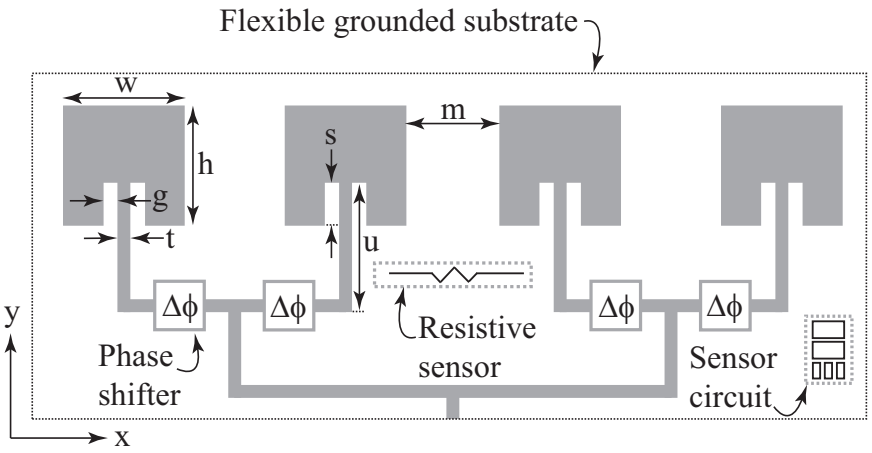

Figure 41. Schematic of the 1 x 4 Self-adapting flexible (SELFLEX) array with embedded sensor circuitry.

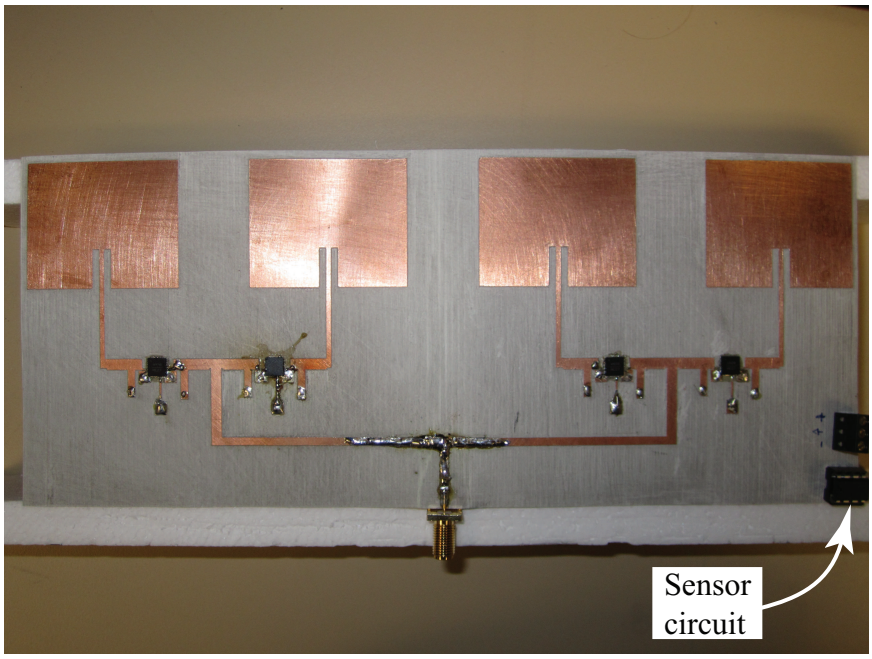

Figure 42. Picture of the manufactured 1 x 4 SELFLEX array prototype (g = 2.0 mm, h = 35.6 mm, m = 19.8 mm, s = 11.0 mm, t = 1.3 mm, u = 33.4 mm and w = 43.6 mm).

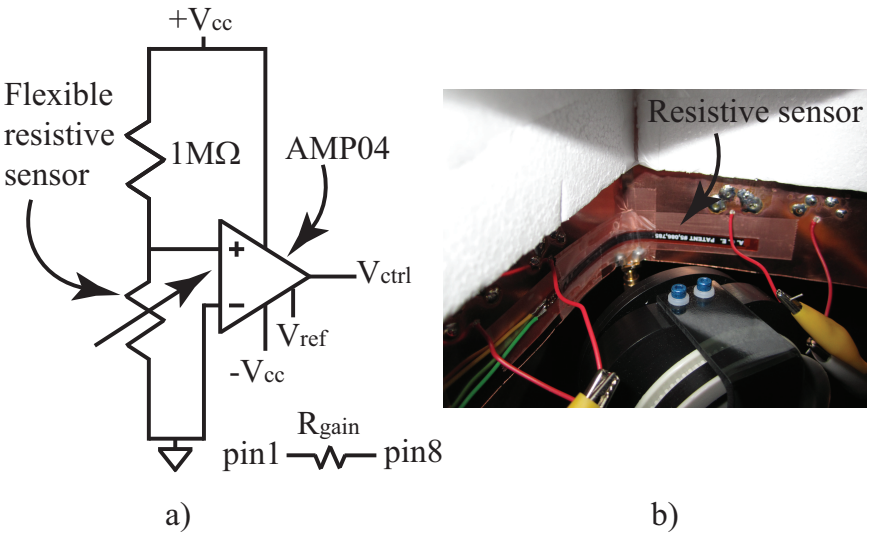

Figure 43. a) Schematic of the sensor circuit used to measure the resistance and control the phase shifters (V_{cc} = 15V, R_{gain}=4.7$k\Omega$ and $V_{ref} = -V_{cc}$ = -0.4V) and b) a picture of the flexible resistive sensor used for measuring surface deformation.

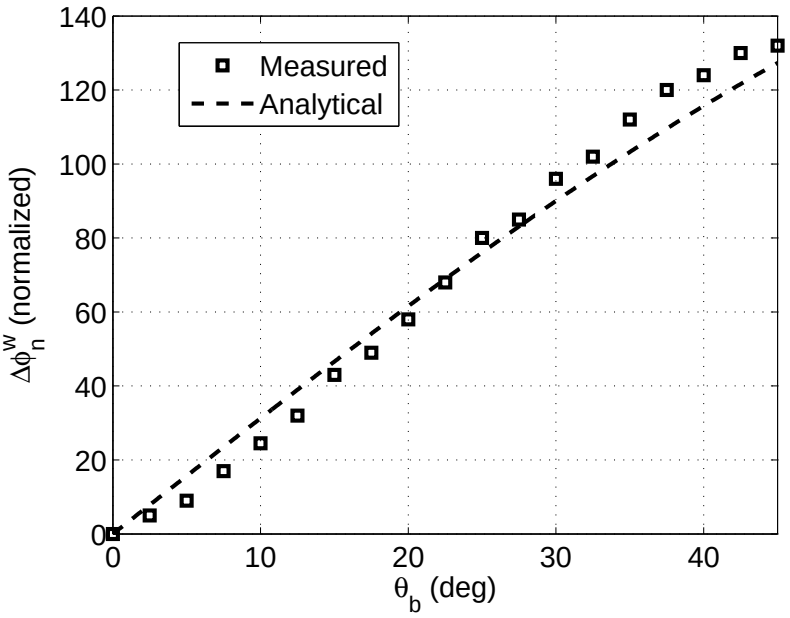

Figure 44. Measured output of the phase shifter controlled by the sensor circuit where θ_b is the bend angle and $\Delta\phi_n^w$ is the phase compensation for the n^{th} antenna element in the array.

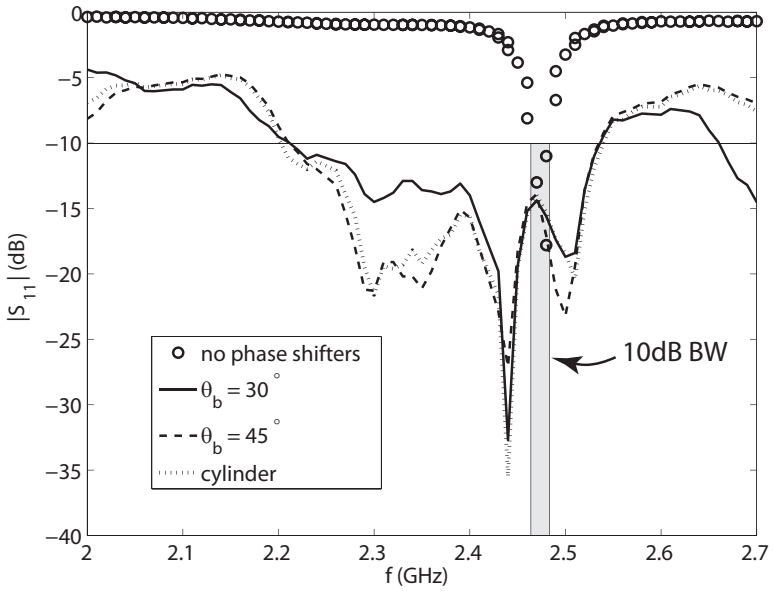

Figure 45. Measured S_{11} of the 1 x 4 SELFLEX array for various conformal surfaces.

application in terms of cost and complexity. With these considerations, a new type of conformal array has been proposed here. The proposed design consists of four microstrip patches. The patches have been printed on a flexible 60 mil thick Rogers RT/duroid 6002 substrate $(\epsilon_r = 2.94, \tan\delta = 0.0012)$ to be operated at 2.47 GHz. To design all the patches on a single surface, microstrip transmission lines have been used as the feed network. The parallel phasor type network, as shown in Fig. 6 a), has been deployed here as a linear feed network. This technique thus eliminates the requirement of multiple feed point to excite the array elements. The details about the geometry of the proposed array can be seen in Fig. 41. The printed prototype is shown in Fig. 42 with phase shifters and the sensor circuit. An image of the flexible resistor attached to the back of the prototype SELFLEX antenna is shown in Fig. 43 b).

4.3. S-parameter and Pattern Measurement Results

The evaluation of the printed SELFLEX array has been performed next by placing the array on a flat surface. The measured return loss S_{11} was recorded for the two designes, with and without the phase shifters. At first, when the array was placed on a flat-surface, there would be no need for the correction of the phases. Considering this situation as the reference position, the S_{11} values of the array with the phase shifters were recorded. As Fig. 45 suggests, a good 10 dB bandwidth centered at 2.46 GHz has been observed.

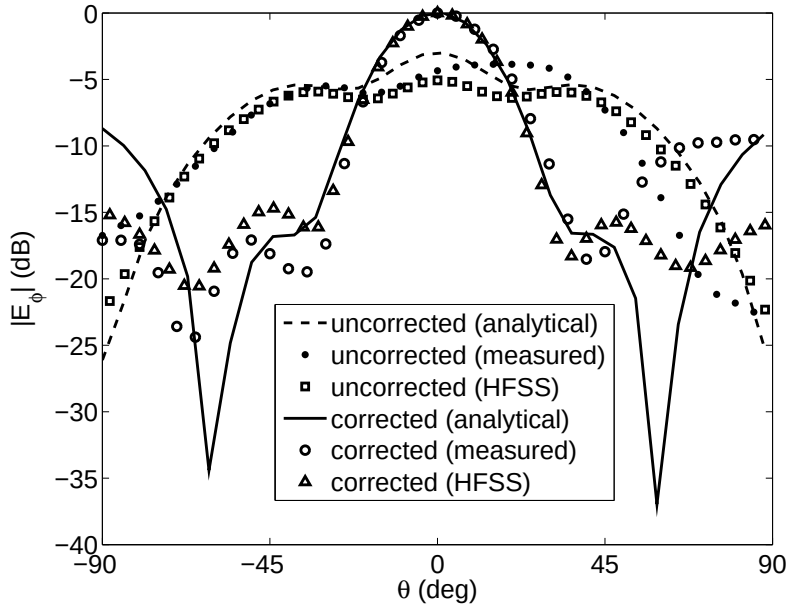

Figure 46. Measured and analytical patterns at 2.47 GHz in the x-z plane for the array with the embedded sensor circuit on a wedge with $\theta_b = 30^\circ$.

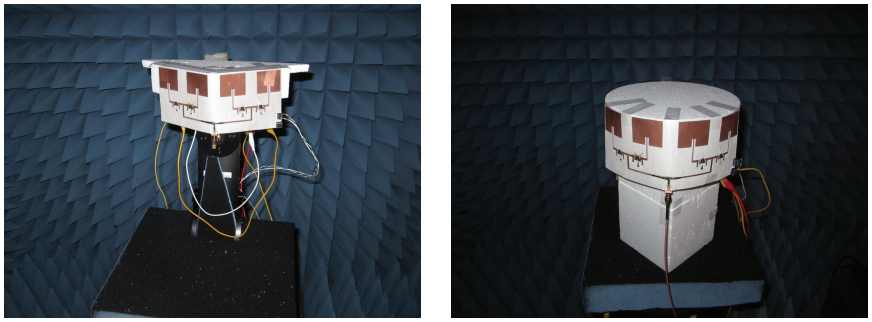

a) b)

Figure 47. a) Picture of the 1 x 4 SELFLEX array attached to a non-conducting wedge and b) picture of the 1 x 4 SELFLEX array attached to a non-conducting cylinder.

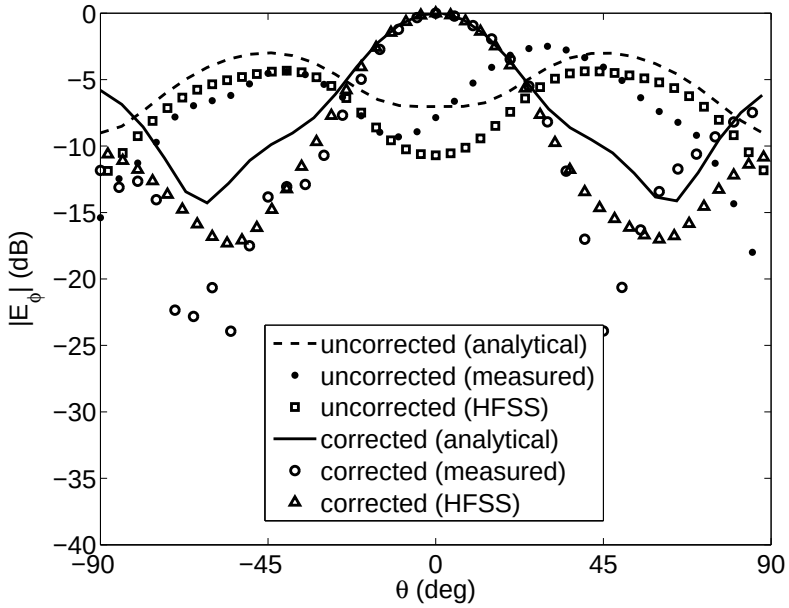

Figure 48. Measured and analytical patterns at 2.47 GHz in the x-z plane for the array with the embedded sensor circuit on a wedge with $\theta_b = 45°$.

4.3.1. Pattern Correction of The Antenna on Wedge-Shaped Surfaces

Next, the array with the phase shifters was attached to a non-conducting wedge-shaped surface in the anechoic chamber and the S-parameter and radiation pattern properties were measured. The test setup for $\theta_b = 30\,°$ can be seen in Fig. 47 a). Then the S_{11} values were measured for the two conditions $\theta_b = 30\,°$ and $45\,°$ and have been plotted in Fig. 45 for comparison with the reference position. Measurements show that a good impedance match at 2.47 GHz has been achieved for both of the bend angles, shown as the gray area in Fig. 45. These S_{11} values were measured when the phase shifters were turned on and working under the control of the sensor circuit autonomously. Next, the radiation pattern measurements in the $x-z$ plane were carried out. For validation, radiation patterns were taken for both compensated and uncompensated cases and compared with not only the analytical computations, using equation (3.1) and equation (3.2) but also the simulation results from Ansys HFSS [51]. The results from these computations and simulations are also shown in Figures 46 and 48 showing good agreement between each observation.

4.3.2. Pattern Correction of The Antenna on Cylindrical Surfaces

The behavior of the conformal array was also studied for a cylindrical surface. To do that, the SELFLEX array was put on a non-conducting cylindrical surface with radius 10 cm in the anechoic

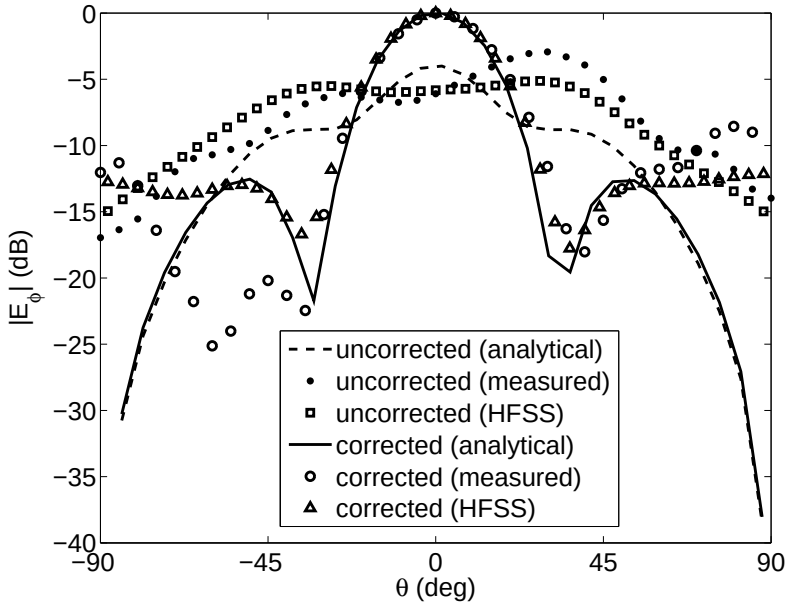

Figure 49. Measured and analytical patterns at 2.47 GHz in the x-z plane for the array with the embedded sensor circuit on a cylinder with a radius of curvature of 10cm.

chamber, as shown in Fig. 47 b). The measured S_{11} values are shown in Fig. 45 illustrating that the SELFLEX antenna has a good match at 2.47 GHz when the phase shifters were working under the control of the sensor circuit autonomously. The radiation pattern for this setup was also recorded and compared with analytical values using equation (2.19) and simulated values from Ansys HFSS [51] on $x-z$ plane at 2.47 GHz, as shown in Fig. 49.

There is an interesting phenomenon occurred for each of the pattern correction cases. In Figures 46, 48 and 49, the radiation patterns are much broader for the uncorrected cases. This can be justified by the results provided by [2] and [22] on circular arrays. As the surface of the conformal array changes from a planar to non-planar orientation, the spacial distribution of the array elements approaches the orientation similar to a circular array. Broadening of the array pattern is therefore expected because of the resemblance of the linear conformal array to a circular array. It should be mentioned that the patterns were also measured in the $y-z$ plane and were similar to the fields from a 1×4 microstrip array. In all cases, good agreement between the measurements and the analytical computations can be observed. A small amount of asymmetries can be seen in all of the measured field patterns with respect to $\theta = 0^{\circ}$ which can be explained as the measurement error due to the limitation of the equipments in chamber.

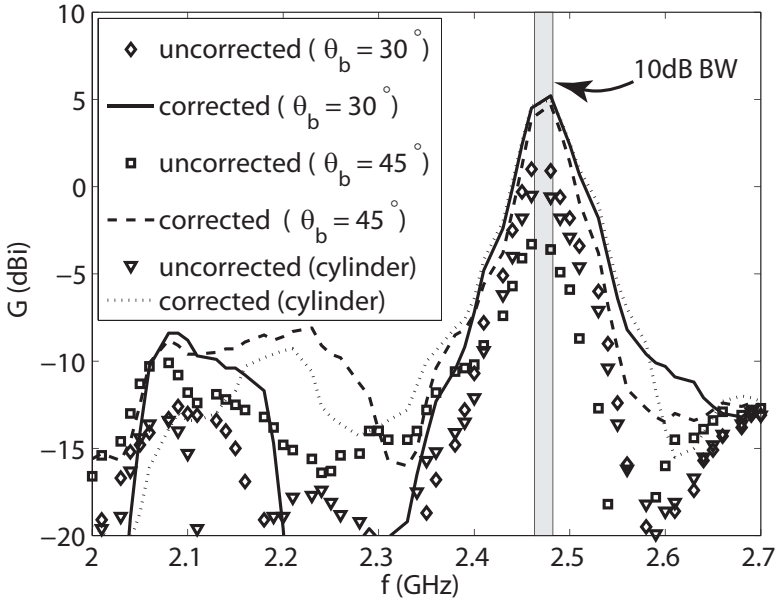

Figure 50. Measured calibrated gain of the 1 x 4 SELFLEX array for various conformal surfaces.

Table 2. Gain Shift Values for the SELFLEX array.

Surface	$G_{s,analy.}$	$G_{s,meas.}$	$G_{s,HFSS}$	Proj. spacing
$\theta_b = 30°$	-0.6 dBi	-0.9 dBi	-0.73	0.43λ
$\theta_b = 45°$	-1.3 dBi	-1.4 dBi	-2.0	0.35λ
Disk	-0.8 dBi	-1.2 dBi	-1.25	non-uniform

4.4. Gain Compensation Results

The calibrated gain values for the SELFLEX design were also measured and the comparison with analytical and simulated gain was shown in Table 2 when the array was placed on the wedge of angle $\theta_b = 30\,^\circ$ and $45\,^\circ$ and on the disk. Finally, an interesting occurrence of multiple resonance points can be observed in Fig. 45. It is believed that this multiple resonance behavior of the conformal array occurrs due to the poor matching of the phase shifter blocks and the variation of the mutual coupling between the elements due to the change in inter-element spacing during the conformal activity of the array. Although the phase shifters do not offer good matching networks and the investigation of mutual coupling due to conformal activity of the array is beyond the scope of current work, still the results in Fig. 50. show that the improvement in the maximum gain is occurring in the 10 dB bandwidth of the array.

CHAPTER 5. CONCLUSIONS

The properties and development of a self-adapting conformal antenna array for wireless communications have been studied in this work. Initially the analytical background related to this work was developed. For validation of the proposed theoretical work, development of a test platform was carried out. This test platform consists of discrete RF blocks and can be used to realize a conformal array at 2.46 GHz. Using the proposed phase compensation methodology, good comparison between measured and analytical results was observed for a general array system. Then a conformal 1×4 microstrip phased antenna array has been developed on a flexible substrate. This new design consists of sensor circuitry that enables the design to autonomously correct its radiation pattern while operating on various non-planar surfaces. This novel SELF-adapting FLEXible antenna design has been denoted as a SELFLEX antenna which thus offers an attractive feature of preserving the field pattern behavior autonomously during conformal surface changes. Finally, throughout this work, measurements are shown to agree well with simulations and analytical computations.

REFERENCES

[1] Lars Josefsson and Patrik Persson, *Conformal Array Antenna Theory and Design,* IEEE Antennas and Propagation Society, Sponsor, John Wiley and Sons, Ltd., Hoboken, New Jersey, 2006.

[2] R. L. Haupt, *Antenna Arrays: A Computational Approach,* John Wiley and Sons, Ltd., Hoboken, New Jersey, 2010.

[3] R. Waterhouse, *Printed Antennas for Wireless Communication,* John Wiley and Sons, Ltd., West Sussex, England, 2007.

[4] F. T. Ulaby, *Fundamentals of Applied Electromagnetics,* Prentice Hall, New Jersey, 2001.

[5] C. A. Balanis, *Antenna Theory,* John Wiley and Sons, Ltd., Hoboken, New Jersey, 2005.

[6] R. C. Hansen, *Phased Array Antennas,* John Wiley and Sons, Inc., New York, NY, 1998.

[7] S. Drabowitch, A. Papiernik, H. Griffith, J. Encinas and B. Smith, *Modern Antennas,* Chapman and Hall, London, 1998.

[8] E. Lier, D. Purdy and G. Kautz, US Patent 6163296, "Calibration and integrated beam control / conditioning system for phased-array antennas," Dec. 19, 2000.

[9] E. Lier, D. Purdy, J. Ashe and G. Kautz, "An On-Board Integrated Beam Conditioning System for Active Phased Array Satellite Antennas," *2000 IEEE Intern. Conf. on Phased Array Systems and Technol.,* May 21-25 2000, Dana Point, CA , pp. 509 - 512.

[10] D. Purdy, J. Ashe, E. Lier, US Patent: 2002/0171583 A1, "System and Method for Efficiently Characterizing the Elements in an Array Antenna," Nov. 21, 2002.

[11] E. Lier, M. Zemlyansky, D. Purdy and D. Farina, "Phased array calibration and characterization based on orthogonal coding: Theory and experimental validation," *2010 IEEE Intern. Sympos. on Phased Array Systems and Technol. (ARRAY),* pp. 271 - 278, Oct. 12 - 15, 2010.

[12] P.L. O'Donovan and A.W. Rudge, "Adaptive control of a flexible linear array," *Electron. Lett.,* vol.9, no.6, pp.121-122, Mar. 22, 1973.

[13] K. Finkenzeller, *RFID Handbook:Fundamentals and Applications in Contactless Smart Cards and Identification*, John Wiley and Sons, West Sussex, England, 2003.

[14] W. L. Stutzman and G. A. Thiele, *Antenna Theory and Design,* 2nd ed., John Wiley and Sons, Inc., New York, NY, 1998.

[15] M. Tanaka and J.-H. Jang, "Wearable mircostrip antenna," *IEEE Antennas and Propagation Society International Symposium,* pp. 704-707, vol. 2, Jun. 22-27, 2003.

[16] P. Salonen, H. Hurme, "Modeling of a fabric GPS antenna for smart clothing," *Proc. IASTED International Conference Modeling and Simulation,* Palm Springs, CA, USA, 2003, pp. 18-23.

[17] P. Salone and H. Hurme, "A novel fabric WLAN antenna for wearable applications," *IEEE Antennas and Propagation Society International Symposium,* Jun. 2003.

[18] C. Hertleer, H. Rogier, L. Vallozzi and L. Van Langenhove, "A Textile Antenna for Off-Body Communication Integrated Into Protective Clothing for Firefighters," *IEEE Transactions on Antennas and Propagation,* pp. 919 - 925, vol. 57, no. 4, Apr. 2009.

[19] Z. Konstas, K. Katsibas and M.M. Tentzeris, "A novel "Green" inkjet-printed monopole antenna topology for concurrent RFID and cellular communications," *IEEE Antennas and Propagation Society International Symposium,* June 1-5, 2009.

[20] T. Karacolak, A.Z. Hood and E. Topsakal, "Design of a Dual-Band Implantable Antenna and Development of Skin Mimicking Gels for Continuous Glucose Monitoring," *IEEE Transactions on Microwave Theory and Techniques,* vol.56, no.4, pp.1001-1008, April 2008

[21] P.L. O'Donovan and A.W. Rudge, "Adaptive control of a flexible linear array," *Electronics Letters,* vol.9, no.6, pp.121-122, Mar. 22, 1973.

[22] D. J. Chung, S. K. Bhattacharya, G. E. Ponchak and J. Papapolymerou, "An 8x8 lightweight flexible multilayer antenna array," *Proc. IEEE Antennas Propag. Soc. Int. Symp. Dig.,* June 1-5, 2009, Charleston, SC.

[23] S. Nikolaou, G. E. Ponchak, J. Papapolymerou and M. M. Tentzeris, "Conformal double exponentially tapered slot antenna (DETSA) on LCP or UWB applications," *IEEE Transactions on Antennas and Propagation,* pp. 1663 - 1669, vol. 54, no. 6, Jun. 2006.

[24] J. - L. Guo and J. - Y. Li, "Pattern synthesis of conformal array antenna in the presence of platform using differential evolution algorithm," *IEEE Transactions on Antennas and Propagation,* pp. 2615 - 2621, vol. 57, no. 9, Sep. 2009.

[25] M. A. Aziz, S. Roy, L. A. Berge, I. Ullah and B. D. Braaten, "A conformal CPW folded slot antenna array printedon a Kapton substrate," *Proceedings of the 2012 European Conference on Antennas and Propagation (EUCAP),* Prague, Czech. Republic, Mar. 2012.

[26] K. Wincza and S. Gruszczynski, "Influence of Curvature Radius on Radiation Patterns in Multibeam Conformal Antennas," *36th European Microwave Conference,* vol., no., pp. 1410-1413, Sept. 10 - 15, 2006.

[27] P. Salonen, Y. Rahmat-Samii, H. Hurme and M. Kivikoski, "Dual-band wearable textile antennas," *IEEE Antennas and Propagation Society International Symposium,* pp. 463-466, vol. 1, Jun. 20-25, 2004.

[28] S. Zhu and R. Langley, "Dual-Band Wearable Textile Antenna on an EBG Substrate," *IEEE Transactions on Antennas and Propagation,* pp. 926 - 935, vol. 57 no. 4, Apr. 2009.

[29] P. Salonen, Y. Rahmat-Samii, M. Schaffrath, and M. Kivikoski, "Effect of textile materials on wearable antenna performance: A case study of GPS antennas," in *Proc. IEEE Antennas Propag. Soc. Int. Symp.,* 2004, vol. 1, pp. 459-462.

[30] T.F. Kennedy, P.W. Fink, P.W., A.W. Chu, N.J. Champagne, G.Y. Lin and M.A. Khayat, M.A., "Body-Worn E-Textile Antennas: The Good, the Low-Mass, and the Conformal", *IEEE Transactions on Antennas and Propagation,* pp. 910 - 918, vol. 57, no. 4, Apr. 2009

[31] F. Declercq, H. Rogier and C. Hertleer, "Permittivity and Loss Tangent Characterization for Garment Antennas Based on a New Matrix-Pencil Two-Line Method," *IEEE Transactions on Antennas and Propagation,* pp. 2548 - 2554, vol. 56, no. 8, Aug. 2008.

[32] M. Klemm and G. Troester, "Textile UWB antennas for wireless body area networks," *IEEE Trans. Antennas Propag.,* vol. 54, pp. 3192-3197, 2006.

[33] P. Salonen, Y. Rahmat-Samii, and M. Kivikoski, "Wearable antennas in the vicinity of human body," in *Proc. IEEE Antennas Propag. Soc. Int. Symp.,* 2004, vol. 1, pp. 467-470.

[34] C. Cibin, P. Leuchtmann, M. Gimersky, R. Vahldieck, and S. Moscibroda, "A flexible wearable antenna," in *Proc. IEEE Antennas Propag. Soc. Int. Symp.,* 2004, vol. 4, pp. 3589-3592.

[35] Y. Byram, Y. Zhou, B. S. Shim, S. Xu, J. Zhu, N. A. Kotov and J. L. Volakis, "E-textile conductors and polymer composites for conformal lightweight antennas," *IEEE Transactions on Antennas and Propagation,* pp. 2732 - 2736, vol. 56, no. 8, Aug. 2010.

[36] D. Psychoudakis, G. Y. Lee, C. - C. Chen and J. L. Volakis, "Estimating diversity for body-worn antennas," *3rd European Conference on Antennas and Propagation (EuCAP),* March 23-27, 2009, Berlin Germany.

[37] J. - S. Roh, Y. - S. Chi, J. - H. Lee, Y. Tak, S. Nam and T. J. Kang, "Embroidered wearable multiresonant folded dipole antenna for RF reception," *IEEE Antennas and Wireless Propagation Letters,* pp. 803 - 806, vol. 9, 2010.

[38] S. E. Morris, Y. Bayram, L. Zhang, Z. Wang, M. Shtein and J. L. Volakis, "High-strength, metalized fibers for conformal load bearing antenna applicaitions," *IEEE Transactions on Antennas and Propagation,* pp. 3458 - 3462, vol. 59, no. 9, Sep. 2011.

[39] Z. Wang, L. Zhang, Y. Bayram and J. L. Volakis, "Multilayer printing of embroidered RF circuits on polymer composites," *Proc. IEEE Antennas Propag. Soc. Int. Symp. Dig.,* July 3 - 8, 2011, Spokane WA.

[40] Rogers Corporation, [online] www.rogerscorp.com.

[41] Mini-Circuits, [online] www.minicircuits.com.

[42] Hittite Microwave Corporation, [online] www.hittite.com.

[43] National Instruments Corporation, [online] www.ni.com.

[44] Advanced Design System (ADS) by Agilent Technologies, [online] www.agilent.com.

[45] Analog Devices, [online] www.analog.com.

[46] Spectra Symbol, [online] www.spectrasymbol.com.

[47] Sunlord Electronics USA, Inc., [online] www.sunlordinc.com.

[48] Texas Instruments Inc., [online] www.ti.com

[49] National Semiconductor, [online] www.national.com

[50] SchmartBoard, Inc., [online] www.schmartboard.com

[51] Ansys Inc., Ansys HFSS, Version 13.0.1, [online] www.ansys.com

APPENDIX. MATLAB CODE

The following
SELFLEX1.m
code was used to generate S_{11} and S_{22} graphs obtained from S-parameters measurements of the attenuators and phase shifters as individual blocks.

The following
SELFLEX2.m
code was used to generate S_{11} and S_{22} graphs obtained from S-parameters measurements of the amplifier as an individual block.

The following
SELFLEX3.m
code was used to generate S_{11} and S_{22} graphs obtained from S-parameters measurements of the power combiner as an individual blocks.

The following
SELFLEX4.m
code was used to generate S_{11} graph obtained from S-parameters measurement of the 1×4 test platform.

The following
SELFLEX5.m
code was used to generate phase shifter output graph obtained from analytical and measured normalized phase shift results from the sensor circuit.

The following
SELFLEX6.m
code was used to generate S_{11} graph obtained from S-parameters measurement of the 1×4 SELFLEX array for various conformal surfaces.

The following
SELFLEX7.m
code was used to generate graphs of phase correction results of the 1×4 SELFLEX array for various conformal surfaces shaped as wedge.

The following
SELFLEX8.m
code was used to generate graphs of phase correction results of the 1×4 SELFLEX array for various conformal surfaces shaped as wedge.

SELFLEX1.m File

```
clc
clear all
S_12_phase_shifter=[data...];
phi_12_phase_shifter=[data...];
S_22_phase_shifter=[data...];
S_12_attenuator=[data...];
phi_12_attenuator=[data...];
S_22_attenuator=[data...];
V_shifter=0:.5:5;
```

```
V_attenuator=[0 1:2:17];
figure;
plot(V_shifter,S_12_phase_shifter,'-o','linewidth',4)
grid on;
xlabel('Volt','FontSize', 30)
ylabel('(dB)','FontSize', 30)
%title('Phase-shifter at 2.45 GHz','FontSize', 30)
axis([0 5 -5 0])
figure;
plot(V_shifter,phi_12_phase_shifter-min(phi_12_phase_shifter),'-o','linewidth',4)
grid on;
xlabel('Volt','FontSize', 30)
ylabel('(deg)','FontSize', 30)
%title('Phase-shifter at 2.45 GHz','FontSize', 30)
figure;
plot(V_shifter,S_22_phase_shifter,'-o','linewidth',4)
grid on;
xlabel('Volt','FontSize', 30)
ylabel('(dB)','FontSize', 30)
%title('Phase-shifter at 2.45 GHz','FontSize', 30)
axis([0 5 -35 0])
figure;
plot(V_attenuator,S_12_attenuator,'-o','linewidth',4)
grid on;
xlabel('Volt','FontSize', 30)
ylabel('(dB)','FontSize', 30)
%title('Attenuator at 2.45 GHz','FontSize', 30)
axis([0 17 -40 0])
figure;
plot(V_attenuator,phi_12_attenuator,'-o','linewidth',4)
grid on;
xlabel('Volt','FontSize', 30)
ylabel('(deg)','FontSize', 30)
%title('Attenuator at 2.45 GHz','FontSize', 30)
axis([0 17 0 200])
figure;
plot(V_attenuator,S_22_attenuator,'-o','linewidth',4)
grid on;
xlabel('Volt','FontSize', 30)
ylabel('(dB)','FontSize', 30)
%title('Attenuator at 2.45 GHz','FontSize', 30)
axis([0 17 -30 0])
```

SELFLEX2.m File

```
clc
clear all
freq=[data...];
S_11=[data...];
S_21=[data...];
figure;
plot(freq,S_11,'linewidth',4)
grid on;
```

```
axis([2.4 2.5 -21.2 -20.2])
xlabel('(GHz)','FontSize', 30)
ylabel('(dB)','FontSize', 30)
figure;
plot(freq,S_21,'linewidth',4)
grid on;
axis([2.4 2.5 6.4 6.9])
xlabel('(GHz)','FontSize', 30)
ylabel('(deg)','FontSize', 30)
```

SELFLEX3.m File

```
clc
clear all
freq=[data...];
S_11=[data...];
S_22=[data...];
S_21=[data...];
figure;
plot(freq,S_11,'linewidth',4)
grid on;
axis([2.4 2.5 -22 -20])
xlabel('(GHz)','FontSize', 30)
ylabel('(dB)','FontSize', 30)
figure;
plot(freq,S_22,'linewidth',4)
grid on;
axis([2.4 2.5 -14 -12])
xlabel('(GHz)','FontSize', 30)
ylabel('(dB)','FontSize', 30)
figure;
plot(freq,S_21,'linewidth',4)
grid on;
axis([2.4 2.5 -6.25 -6.05])
xlabel('(GHz)','FontSize', 30)
ylabel('(deg)','FontSize', 30)
```

SELFLEX4.m File

```
clc
clear all
S11=[data...];
pts = 1:10:length(S11);
figure
plot(S11(pts,1)./1e9,S11(pts,2))
axis([2 3 -30 0])
xlabel('f (GHz)')
ylabel('|S_{11}| (dB)')
```

SELFLEX5.m File

```
clc
clear all
angle = 0:2.5:45;
```

```
V=[data...];
offset = .2;
figure
plot(angle,V+offset,'s-')
xlabel('\theta_b')
ylabel('V_{ctrl}')
grid on
axis([0 45 1.5 4.5])
f = 2.44e9;
c = 2.99e8;
lambda = c/f;
k = 2*pi/lambda;
d = lambda/2;
phi = 0:.001:pi;
delta = -k*d*sin(phi);
figure
delta_meas=[data...];
theta_b=0:2.5:45;
plot(theta_b,delta_meas,'s',phi*180/pi,abs(delta*180/pi),'--')
axis([0 45 0 140])
xlabel('\theta_b (deg)')
ylabel('\Delta\phi_n^w (normalized)')
legend('Measured','Analytical')
grid on
```

SELFLEX6.m File

```
clc
clear all
S11_flat=[data...];
figure
pts=1:17:length(S11_30_deg(:,1));
pts2=1:10:length(S11_flat(:,1));
plot(S11_flat(pts2,1)./1e9, S11_flat(pts2,2), 'o', ...
    S11_30_deg(pts,1)./1e9,S11_30_deg(pts,2),'-', ...
    S11_45_deg(pts,1)./1e9,S11_45_deg(pts,2),'--', ...
    S11_disk(pts,1)./1e9,S11_disk(pts,2),':')
xlabel('f (GHz)')
ylabel('|S_{11}| (dB)')
legend('no phase shifters','\theta_b = 30^...
{\circ}','\theta_b = 45^{\circ}','cylinder')
% title('1 x 4 array controlled with the sensor circuit')
axis([2.0 2.7 -40 0])
```

SELFLEX7.m File

```
clc
clear all
S11_flat=[data...];
S11_corrected_30=[data...];
S11_uncorrected_30=[data...];
S11_corrected_45=[data...];
S11_uncorrected_45=[data...];
S12_phase_shifters_flat=[data...];
```

```
S12_corrected_30=[data...];
S12_uncorrected_30=[data...];
S12_corrected_45=[data...];
S12_uncorrected_45=[data...];
E_total_30_uncorrected(:,1)=[data...];
E_phi_bent_30_uncorrected_analytical=[data...];
E_phi_bent_30_corrected_analytical=[data...];
E_phi_bent_30_uncorrected_measured=[data...];
E_phi_bent_30_corrected_measured=[data...];
E_total_30_corrected=[data...];
E_total_45_uncorrected(:,1)=[data...];
E_phi_bent_45_uncorrected_analytical=[data...];
E_phi_bent_45_corrected_analytical=[data...];
E_phi_bent_45_uncorrected_measured=[data...];
E_phi_bent_45_corrected_measured=[data...];
E_total_45_corrected=[data...];
figure
pts=1:20:length(S11_corrected_30);
plot(S11_uncorrected_30(pts,1)./1e9, ...
S11_uncorrected_30(pts,2),'--', ...
    S11_corrected_30(pts,1)./1e9, ...
S11_corrected_30(pts,2),'-', ...
    S11_uncorrected_45(pts,1)./1e9, ...
S11_uncorrected_45(pts,2),'s', ...
    S11_corrected_45(pts,1)./1e9, ...
S11_corrected_45(pts,2),'x', ...
    S11_flat(pts,1)./1e9,S11_flat(pts,2),'o-');
xlabel('f (GHz)')
ylabel('|S_{11}| (dB)')
legend('uncorrected (\theta_b = 30)','...
corrected (\theta_b = 30)', ...
    'uncorrected (\theta_b = 45)','...
corrected (\theta_b = 45)', 'flat')
figure

plot(S12_phase_shifters_flat(pts,1)./...
1e9, S12_phase_shifters_flat(pts,2), 'o', ...
    S12_uncorrected_30(pts,1)./1e9, ...
S12_uncorrected_30(pts,2),'d', ...
    S12_corrected_30(pts,1)./1e9, ...
S12_corrected_30(pts,2),'-', ...
    S12_uncorrected_45(pts,1)./1e9, ...
S12_uncorrected_45(pts,2),'s', ...
    S12_corrected_45(pts,1)./1e9, ...
S12_corrected_45(pts,2),'--');
xlabel('f (GHz)')
ylabel('|S_{12}| (dB)')
legend('flat (\theta_b = 0^{\circ})', ...
    'uncorrected (\theta_b = 30^{\circ})','...
corrected (\theta_b = 30^{\circ})', ...
    'uncorrected (\theta_b = 45^{\circ})','...
corrected (\theta_b = 45^{\circ})')
```

```
figure
pts2=1:2:length(E_total_45_uncorrected(:,1));
plot(180/pi*[-pi/2:.1:pi/2].',20*log10(abs...
(E_phi_bent_45_uncorrected_analytical(:,1))./...
max(abs(E_phi_bent_45_corrected_analytical(:,1)))),'--', ...
     E_phi_bent_45_uncorrected_measured(:,1)...
+-5,20*log10(E_phi_bent_45_uncorrected_measured...
(:,2)./max(E_phi_bent_45_corrected_measured(:,2))),'.', ...
     E_total_45_uncorrected(pts2,1),20*log10...
(E_total_45_uncorrected(pts2,2)./max...
(E_total_45_corrected(pts2,2))), 's', ...
     180/pi*[-pi/2:.1:pi/2].',20*log10(abs...
(E_phi_bent_45_corrected_analytical(:,1))./...
max(abs(E_phi_bent_45_corrected_analytical(:,1)))),'-', ...
     E_phi_bent_45_corrected_measured(:,1)+-5,20*log10...
(E_phi_bent_45_corrected_measured(:,2)./max...
(E_phi_bent_45_corrected_measured(:,2))),'o', ...
      E_total_45_corrected(pts2,1),20*log10...
(E_total_45_corrected(pts2,2)./max...
(E_total_45_corrected(pts2,2))), '^')



legend('uncorrected (analytical)',...
    'uncorrected (measured)',...
    'uncorrected (HFSS)', ...
'corrected (analytical)', ...
'corrected (measured)', ...
'corrected (HFSS)')
axis([-90 90 -40 0])
title('x-z plane - 1 x 4 array controlled with the sensor ...
circuit on a wedge with \theta_b=45')
xlabel('\theta (deg)')
ylabel('|E_{\phi}| (dB)')

figure
plot(180/pi*[-pi/2:.1:pi/2].',20*log10(abs...
(E_phi_bent_30_uncorrected_analytical...
(:,1))./max(abs(E_phi_bent_30_corrected_...
analytical(:,1)))),'--', ...
     E_phi_bent_30_uncorrected_measured(:,1)...
+-5,20*log10(E_phi_bent_30_uncorrected_measured...
(:,2)./max(E_phi_bent_30_corrected_measured(:,2))),'.', ...
     E_total_30_uncorrected(pts2,1),20*log10...
(E_total_30_uncorrected(pts2,2)./max...
(E_total_30_corrected(pts2,2))), 's', ...
    180/pi*[-pi/2:.1:pi/2].',20*log10(abs...
(E_phi_bent_30_corrected_analytical(:,1))./...
max(abs(E_phi_bent_30_corrected_analytical(:,1)))),'-', ...
 E_phi_bent_30_corrected_measured(:,1)...
+-5,20*log10(E_phi_bent_30_corrected_measured...
```

```
(:,2)./max(E_phi_bent_30_corrected_measured(:,2))),'o', ...
      E_total_30_corrected(pts2,1),20*log10...
(E_total_30_corrected(pts2,2)./max...
(E_total_30_corrected(pts2,2))), '^')


axis([-90 90 -40 0])

legend('uncorrected (analytical)',...
    'uncorrected (measured)',...
    'uncorrected (HFSS)', ...
'corrected (analytical)', ...
'corrected (measured)', ...
'corrected (HFSS)')

title('x-z plane - 1 x 4 array controlled with the sensor ...
circuit on a wedge with \theta_b=30')
xlabel('\theta (deg)')
ylabel('|E_{\phi}| (dB)')

figure
polar(pi/180*E_phi_bent_45_corrected_measured...
(:,1)+-5*pi/180,E_phi_bent_45_corrected_measured...
(:,2)./max(E_phi_bent_45_corrected_measured(:,2)),'.-')
hold on
polar(pi/180*E_phi_bent_45_uncorrected_measured...
(:,1)+-5*pi/180,E_phi_bent_45_uncorrected_measured...
(:,2)./max(E_phi_bent_45_corrected_measured(:,2)),'x-')
polar([-pi/2:.1:pi/2].',abs(E_phi_bent_45_uncorrected_analytical...
(:,1))./max(abs(E_phi_bent_45_corrected_analytical(:,1))),'--')
polar([-pi/2:.1:pi/2].',abs(E_phi_bent_45_corrected_analytical...
(:,1))./max(abs(E_phi_bent_45_corrected_analytical(:,1))),'-')
xlabel('\theta_b = 45 (deg)')
title('x-z plane - 1 x 4 array controlled with the sensor ...
circuit on a wedge')
```

SELFLEX8.m File

```
clc
clear all
S11_flat=[];
S11_uncorrected=[];
S12_uncorrected=[];
S11_corrected=[];
S12_corrected=[];
S12_array=[];
E_phi_r_10cm_corrected_measured=[];
E_phi_r_10cm_uncorrected_measured=[];
E_phi_r_10cm_corrected_analytical=[];
E_phi_r_10cm_uncorrected_analytical=[];
E_total_uncorrected=[];
E_total_corrected=[];
```

```
pts2=1:2:length(E_total_uncorrected(:,1));
theta = [-pi/2:.1:pi/2]'*180/pi;
figure
plot(theta,20*log10...
(abs(E_phi_r_10cm_uncorrected_analytical)./
max(abs(E_phi_r_10cm_corrected_analytical))),'--', ...
    E_phi_r_10cm_uncorrected_measured(:,1),20*log10...
(E_phi_r_10cm_uncorrected_measured(:,2)./...
max(E_phi_r_10cm_corrected_measured(:,2))),'.', ...
     E_total_uncorrected(pts2,1),...
20*log10(E_total_uncorrected(pts2,2)./...
max(E_total_corrected(pts2,2))), 's', ...
    theta,20*log10(abs...
(E_phi_r_10cm_corrected_analytical)./...
max(abs(E_phi_r_10cm_corrected_analytical))),'-', ...
E_phi_r_10cm_corrected_measured(:,1)-5,20*log10...
(E_phi_r_10cm_corrected_measured(:,2)/...
max(E_phi_r_10cm_corrected_measured(:,2))),'o', ...
     E_total_corrected(pts2,1),20*log10...
(E_total_corrected(pts2,2)./max...
(E_total_corrected(pts2,2))), '^')

xlabel('\theta (deg)')
ylabel('|E_{\phi}| (dB)')
axis([-90 90 -40 0])
title('x-z plane - 1 x 4 array controlled ...
with the sensor circuit on a 10 cm disk')

legend('uncorrected (analytical)',...
    'uncorrected (measured)',...
    'uncorrected (HFSS)', ...
'corrected (analytical)', ...
'corrected (measured)', ...
'corrected (HFSS)')
```